

Global deposition of total reactive nitrogen oxides from 1996 to 2014 constrained with satell...

This work was made openly accessible by BU Faculty. Please [share](#) how this access benefits you. Your story matters.

Version	Published version
Citation (published version):	Jeffrey A Geddes, Randall V Martin. "Global deposition of total reactive nitrogen oxides from 1996 to 2014 constrained with satellite observations of NO2 columns." Atmospheric Chemistry and Physics Discussions, pp. 1 - 44. https://doi.org/10.5194/acp-2016-1100

<https://hdl.handle.net/2144/31483>

Boston University



1 **Global deposition of total reactive nitrogen oxides from**
2 **1996 to 2014 constrained with satellite observations of NO₂**
3 **columns**

4
5 **Jeffrey A. Geddes^{1,2}, Randall V. Martin^{1,3}**

6 (1){Department of Physics and Atmospheric Science, Dalhousie University, Halifax, Nova
7 Scotia, Canada}

8 (2){Now at: Department of Earth and Environment, Boston University, Boston,
9 Massachusetts, USA}

10 (3){Harvard-Smithsonian Center for Astrophysics, Cambridge, Massachusetts, USA}

11 Correspondence to: J.A. Geddes (jgeddes@bu.edu)

12

13 **Abstract**

14 Reactive nitrogen oxides (NO_y) are a major constituent of the nitrogen deposited from the
15 atmosphere, but observational constraints on their deposition are limited by poor or
16 nonexistent measurement coverage in many parts of the world. Here we apply NO₂
17 observations from multiple satellite instruments (GOME, SCIAMACHY, and GOME-2) to
18 constrain the global deposition of NO_y over the last two decades. We accomplish this by
19 producing top-down estimates of NO_x emissions from inverse modeling of satellite NO₂
20 columns over 1996-2014, and including these emissions in the GEOS-Chem chemical
21 transport model to simulate chemistry, transport, and deposition of NO_y. Our estimates of
22 long-term mean wet nitrate (NO₃⁻) deposition are highly consistent with available
23 measurements in North America, Europe, and East Asia combined ($r = 0.83$, normalized mean
24 bias = -7%, $N = 136$). Likewise, our calculated trends in wet NO₃⁻ deposition are largely
25 consistent with the measurements, with 129 of the 136 gridded model-data pairs sharing
26 overlapping 95% confidence intervals. We find that global mean NO_y deposition over 1996-
27 2014 is 56.0 Tg N yr⁻¹, with a minimum in 2006 of 50.5 Tg N and a maximum in 2012 of 60.8
28 Tg N. Regional trends are large, with opposing signs in different parts of the world. Over
29 1996 to 2014, NO_y deposition decreased by up to 60% in eastern North America, doubled in



1 regions of East Asia, and declined by 20% in parts of Western Europe. About 40% of the
2 global NO_y deposition occurs over oceans, with deposition to the North Atlantic Ocean
3 declining and deposition to the northwestern Pacific Ocean increasing. Using the residual
4 between NO_x emissions and NO_y deposition over specific land regions, we investigate how
5 NO_x export via atmospheric transport has changed over the last two decades. Net export from
6 the continental United States decreased substantially, from 2.9 Tg N yr^{-1} in 1996 to 1.5 Tg N
7 yr^{-1} in 2014. On the other hand, export from China more than tripled between 1996 and 2011
8 (from 1.0 Tg N yr^{-1} to 3.5 Tg N yr^{-1}), before a striking decline to 2.5 Tg N yr^{-1} by 2014. We
9 find that declines in NO_x export from some Western European countries have counteracted
10 increases in emissions from neighbouring countries to the east. A sensitivity study indicates
11 that simulated NO_y deposition is robust to uncertainties in NH_3 emissions with a few
12 exceptions. Our novel long-term study provides timely context on the rapid redistribution of
13 atmospheric nitrogen transport and subsequent deposition to ecosystems around the world.

14

15 **1 Introduction**

16 The introduction of reactive nitrogen to the environment by anthropogenic activities (e.g.
17 from fossil fuel combustion and the production of fertilizers for agriculture) has drastically
18 altered the global nitrogen cycle with consequences throughout the Earth system (Galloway
19 2004). Reactive nitrogen dominates the chemical production of tropospheric ozone and
20 contributes to inorganic aerosol formation, with implications for air quality and climate.
21 Deposition of nitrogen from the atmosphere has been linked to eutrophication and
22 acidification (Bouwman et al., 2002), reductions in biodiversity (Bobbink et al., 2010;
23 Hernández et al., 2016; Isbell et al., 2013; De Schrijver et al., 2011), and climate impacts
24 through coupling with the carbon cycle and greenhouse gas emissions (Liu and Greaver,
25 2009; Reay et al., 2008; Templer et al., 2012). Despite its global importance, observational
26 constraints on nitrogen deposition are lacking in many parts of the world due to poor or
27 nonexistent measurement coverage (Vet et al., 2014).

28 Atmospheric transport is a dominant process for distributing reactive nitrogen around the
29 world (Galloway et al., 2008). Some forms of reactive nitrogen can be transported over
30 distances greater than 1000 km (Neuman et al., 2006; Sanderson et al., 2008), depositing
31 across national boundaries and continents. For example, the U.S. is estimated to export 30-
32 40% of its reactive nitrogen emissions (Dentener et al., 2006; Holland et al., 2005; Zhang et



1 al., 2012), while transport from China accounts for up to 66-92% of total nitrogen deposition
2 to parts of the northwestern Pacific Ocean (Zhao et al., 2015). Fertilization of the open ocean
3 due to atmospheric transport and deposition of anthropogenic nitrogen may be a considerable
4 factor in marine productivity (Duce et al., 2008), prompting important questions about the fate
5 and impact of deposition far downwind of sources where observations are limited.

6 Reactive nitrogen oxides ($\text{NO}_y \equiv \text{NO} + \text{NO}_2 + \text{HNO}_3 + \text{HONO} + \text{organic nitrate}$
7 molecules + aerosol nitrate) contribute about half of the total nitrogen deposited worldwide
8 (Dentener et al., 2006). NO_y deposition was estimated to be around 45-50 Tg N yr^{-1} in the
9 late-1990s and early 2000s, representing a 3-4 fold increase since the pre-industrial era
10 (Dentener et al., 2006; Kanakidou et al., 2016; Lamarque et al., 2013). A substantial range
11 exists in the trajectory of global NO_y deposition beyond the year 2000 depending on emission
12 scenario. Galloway et al. (2004) projected that NO_y deposition could increase by >70% by
13 2050, while Dentener et al. (2006) projected changes between -25% to +50% by 2030 for
14 maximum feasible reduction and “pessimistic” scenarios respectively. More recent multi-
15 model projections by Lamarque et al. (2013) estimate NO_y deposition would change by -16%
16 to +5% for 2030 and by -48% to -25% for 2100, depending on the Representative
17 Concentration Pathway (RCP) scenario. This range in projections highlights the need for the
18 global observational constraints on contemporary changes in nitrogen oxide emissions.

19 Sources of NO_x ($\equiv \text{NO} + \text{NO}_2$), whose oxidation is responsible for the formation of other
20 reactive nitrogen oxides, include fossil fuel combustion, biomass burning, lightning, and
21 biogenic emission from soil. The magnitude and spatial distribution of NO_x emissions have
22 changed considerably over the past several decades, corresponding to patterns of human
23 development and emission control measures. Tropospheric NO_2 columns derived from
24 satellite remote sensing observations have been used extensively to constrain regional and
25 global NO_x emissions (Streets et al., 2013). This top-down approach complements bottom-up
26 inventories that are assembled using regionally specific emission factors and fuel combustion
27 data for various source categories. In particular, satellite NO_2 observations can provide insight
28 into otherwise poorly constrained sources (Beirle et al., 2010; Jaegle et al., 2005; Richter et
29 al., 2004; Vinken et al., 2014), produce coherent long-term trends (van der A et al., 2008; Lu
30 et al., 2015; Stavroukou et al., 2008; Zhang et al., 2007), document interannual variability
31 (Castellanos and Boersma, 2012; Kononov et al., 2010; Russell et al., 2012), offer
32 information to evaluate and improve bottom-up inventories at the global scale (Martin, 2003;



1 Miyazaki et al., 2016), and provide timely emission updates (Lamsal et al., 2011; Mijling et
2 al., 2013; Sourì et al., 2016).

3 Satellite observations of NO₂ began with GOME (1995-2003) followed by
4 SCIAMACHY (2002-2011), and continue today with OMI (2004-), GOME-2 (2007-), and
5 TROPOMI (2017-), resulting in a record of global atmospheric NO₂ abundance over the past
6 20 years. These observations have been used previously to estimate the deposition of nitrogen
7 species, either in combination with chemical transport modeling or with empirical approaches
8 (Cheng et al., 2013; Jia et al., 2016; Lu et al., 2013; Nowlan et al., 2014). For example,
9 Nowlan et al. (2014) demonstrated how satellite-inferred surface concentrations of NO₂ can
10 be combined with modeling to produce spatially continuous estimates of NO₂ dry deposition
11 fluxes.

12 In this study, we expand on the approach of Nowlan et al. (2014) by using the satellite
13 observations of NO₂ columns to constrain total NO_y deposition, including other oxidized
14 nitrogen species and wet deposition which contribute substantially to NO_y deposition. We
15 accomplish this by constraining surface NO_x emissions using the satellite observations of
16 NO₂, and simulating subsequent NO_y deposition with a global chemical transport model.
17 Given the effective mass balance between NO_x emissions and deposition of reactive nitrogen
18 oxides, observational constraints on NO_x emissions provide a powerful top-down constraint
19 on deposition (which to our knowledge has not yet been exploited in this way).

20 We leverage the long-term coverage of GOME, SCIAMACHY, and GOME-2
21 observations to produce a globally consistent and continuous record of NO_y deposition from
22 1996 to 2014. We highlight long-term trends in satellite-constrained NO_y deposition around
23 the world and discuss changes in regional export of NO_x. Our satellite-constrained estimates
24 of NO_y deposition are evaluated using measured wet nitrate (NO₃⁻) deposition from a variety
25 of sources worldwide. We also explore the sensitivity of the NO_y deposition estimates to
26 uncertainties in NH₃ emissions.

27



1 **2 Methods**

2 **2.1 Satellite-based constraints on NO_y deposition**

3 The application of satellite NO₂ column observations to constrain NO_y deposition
4 requires a method to propagate the observational information across the entire NO_y system
5 containing species with lifetimes of days or longer. The short NO_x lifetime of hours during
6 daytime satellite observations implies that a direct assimilation for NO₂ column abundance
7 would rapidly lose the observational information as the assimilation returns to its unperturbed
8 state well before the next satellite observation days later. We therefore apply satellite NO₂
9 observations to constrain NO_x emissions in a simulation of NO_y deposition so the information
10 propagates across the entire NO_y system.

11 We calculate top-down surface NO_x emissions from 1996 to 2014 using observations
12 from GOME (1995-2003), SCIAMACHY (2002-2011) and GOME-2 (2007-). The similar
13 overpass time of these three instruments facilitates their combination to provide consistent
14 long-term coverage (Geddes et al., 2015; Hilboll et al., 2013). Tropospheric NO₂ vertical
15 column densities are provided by KNMI at <http://www.temis.nl/airpollution/>. In all cases,
16 NO₂ column densities are retrieved by differential optical absorption spectroscopy using
17 backscattered radiance in the 425-450 nm wavelength range according to the retrieval
18 algorithm documented in Boersma et al. (2004). Boersma et al. (2016) well describe the value
19 of accounting for vertically-resolved instrument sensitivity. We use the averaging kernels
20 provided with the data to replace a priori NO₂ vertical profiles with those from GEOS-Chem
21 model following Lamsal et al. (2010). We use daily nadir observations with a cloud radiance
22 fraction of less than 0.5. We minimize errors associated with wintertime retrievals by using a
23 solar zenith angle cut-off of 50°.

24 We use the GEOS-Chem chemical transport model (www.geos-chem.org) v9-02 to
25 conduct the inversion of satellite observations of NO₂ and constrain global NO_y deposition.
26 The simulation is described in Appendix 1. Briefly, GEOS-Chem is driven by assimilated
27 meteorology from the NASA Global Modeling and Assimilation Office and simulates
28 detailed HO_x-NO_x-VOC-aerosol chemistry (Bey et al., 2001; Park et al., 2004). Removal
29 occurs through wet deposition (Amos et al., 2012; Liu et al., 2001), and dry deposition based
30 on the widely used resistance-in-series formulation (Wesely, 1989). Anthropogenic, biogenic,
31 soil, lightning, and biomass burning emissions are included (see Appendix 1). In the case of



1 NO_x, the bottom-up emissions are used as prior estimates that we then overwrite with the top-
2 down emissions.

3 We adopt a finite-difference mass balance inversion (Lamsal et al., 2011; Cooper et al.,
4 *submitted*) for computational expedience given the 19-year period of interest. In two initial
5 simulations, a perturbation (30%) to the a-priori emissions, E , in a grid cell is used to find the
6 relationship between the a-priori NO₂ column, Ω , and the change in the column resulting from
7 that perturbation:

$$8 \quad \frac{\Delta E}{E} = \beta \times \frac{\Delta \Omega}{\Omega} \quad (1)$$

9 The factor β in Equation 1 accounts for non-linear feedbacks between a change in NO_x
10 emissions and NO_x chemistry in a grid cell leading to grid cell NO₂ column abundance.

11 We then use monthly-mean gridded satellite observations, Ω_{sat} , in combination with
12 monthly β values for each grid box to derive new gridded annual emissions, $E_{topdown}$, from the
13 prior emissions estimates, E_{prior} , by rewriting Equation 1 as:

$$14 \quad E_{topdown} = E_{prior} \cdot \left[1 - \beta \frac{\Omega_{sat} - \Omega_{prior}}{\Omega_{prior}} \right] \quad (2)$$

15 In all cases, monthly mean simulated NO₂ columns are calculated using days with coincident
16 satellite observations. We calculate annual mean scaling factors from the mean monthly top-
17 down emissions. The top-down emissions are then used in a final simulation. For locations
18 without satellite observations, the a-priori emissions are used. The resultant simulation of NO_y
19 deposition is thus constrained by, and consistent with, the satellite NO₂ observations (similar
20 in essence to an assimilation system). We note uncertainty in tropospheric NO₂ from lightning
21 will propagate into the inversion (Travis et al. 2016), but there is no evidence of a significant
22 trend in lightning NO_x over the long term (Murray et al. 2012). A constant bias is unlikely to
23 affect the trend analyses presented here.

24 We derive global mean satellite-constrained NO_x emissions from 1996-2014 of $53.2 \pm$
25 3.4 Tg N yr⁻¹. Our top-down global NO_x emissions for 2001 of 50.0 Tg N are consistent with
26 the mean \pm standard deviation from over 20 models used in the Coordinated Model Studies
27 Activities of the Task Force on Hemispheric Transport of Air Pollution (HTAP) for the same
28 year of 46.6 ± 7.8 Tg N (Vet et al. 2014).



1 2.2 Measurements of Wet Deposition

2 We use a variety of regional and global measurements of wet nitrate (NO_3^-) deposition
3 to evaluate our satellite-constrained simulation from 1996 to 2014.

4 To evaluate overall global performance we use data compiled by the World Data Centre
5 for Precipitation Chemistry for two time periods: 2000-2002 and 2005-2007
6 (<http://www.wdpc.org/>). The use of this data ensures optimal and consistent quality
7 standards across all stations, allowing for evaluation of global performance with careful
8 consideration of sampling protocols and data completeness (Vet et al. 2014).

9 To evaluate the long-term means and trends from 1996-2014, we obtain observations of
10 wet NO_3^- deposition from North America, Europe, and East Asia where continuous
11 measurements are available throughout most of our study period. Observations come from the
12 National Atmospheric Deposition Program in the United States (<http://nadp.sws.uiuc.edu/>,
13 available 1996-2014), from the Canadian Air and Precipitation Monitoring Network in
14 Canada (<http://www.ec.gc.ca/rs-mn/>, available 1996-2011), from the European Monitoring
15 and Evaluation Programme in Europe (<http://www.emep.int/>, available 1996-2014) and from
16 the Acid Deposition Monitoring Network in East Asia (<http://www.eanet.asia>, available 2000-
17 2014). In the US and Canada, wet deposition is measured by wet-only samplers that are
18 triggered at the onset of precipitation. Measurements in Europe are made by bulk- and wet-
19 only sampling methods and we used both in this analysis. Measurements across East Asia are
20 reported as wet-only, although at some stations this may not be accomplished by strictly wet-
21 only samplers (<http://www.eanet.asia/product/manual/prev/techwet.pdf>).

22 For our analysis, we only included stations which had quality controlled annual data for
23 at least 15 of the 19 years in our study. This left 128 stations across the United States, 14
24 stations in Canada, 18 stations across Europe, and 14 stations across East Asia. For
25 comparison with the GEOS-Chem model, if multiple stations are available within a single
26 grid box we grid all measurements of annual wet deposition to the model horizontal
27 resolution.

28

29 3 Satellite-Constrained Estimates of NO_y Deposition

30 Here we summarize the overall patterns in long-term mean deposition resulting from our
31 satellite-constrained simulation, followed by a discussion of the long term trends, changes in



1 regional export, and the sensitivity of the simulated NO_y deposition to potential uncertainties
2 in NH_3 emissions.

3 **3.1 Long-term Mean NO_y Deposition**

4 Figure 1 (top) shows our satellite-constrained long-term mean NO_y deposition from
5 1996 to 2014. We find that $32.2 \text{ Tg N yr}^{-1}$ is deposited on average over the continents (57% of
6 the total), and $23.8 \text{ Tg N yr}^{-1}$ is deposited on average over the oceans (43% of the total). This
7 is similar to the estimate by Galloway et al. (2004) that 46% of modern day NO_y deposition
8 occurs over the oceans. Critical nitrogen deposition loads for various natural freshwater and
9 terrestrial ecosystems lie in the range of $5\text{--}20 \text{ kg N ha}^{-1} \text{ yr}^{-1}$, depending on the ecosystem, soil
10 conditions, and land history (World Health Organization, 2000). We estimate that mean
11 deposition of oxidized nitrogen alone exceeds $5 \text{ kg N ha}^{-1} \text{ yr}^{-1}$ over a land area of
12 approximately $12.7 \times 10^6 \text{ km}^2$ (or ~8% total land area).

13 In the Northern Hemisphere, high NO_y deposition tends to be associated with regions
14 that have high anthropogenic NO_x sources. We find mean NO_y deposition in the eastern
15 United States exceeds $10 \text{ kg N ha}^{-1} \text{ yr}^{-1}$ (maximum = $11.4 \text{ kg N ha}^{-1} \text{ yr}^{-1}$) with elevated
16 deposition extending into southeastern Canada and hundreds of kilometers into the Atlantic
17 Ocean. This is similar to the multi-model ensemble results from ACCMIP and HTAP,
18 predicting between $5\text{--}15 \text{ kg N ha}^{-1} \text{ yr}^{-1}$ in this region (Lamarque et al. 2013; Vet et al. 2014).
19 A prior GEOS-Chem analysis over North America for the years 2006–2008 also predicted
20 NO_y deposition exceeding $10 \text{ kg N ha}^{-1} \text{ yr}^{-1}$ in the eastern US (Zhang et al. 2012). Elsewhere
21 in North America, we find high NO_y deposition along the west coast of California (up to 6 kg
22 $\text{N ha}^{-1} \text{ yr}^{-1}$) and in the vicinity of Mexico City (up to $10 \text{ kg N ha}^{-1} \text{ yr}^{-1}$).

23 We find mean NO_y deposition is also elevated throughout Europe, with a maximum of
24 $8.5 \text{ kg N ha}^{-1} \text{ yr}^{-1}$ located in northern Italy near the Po Valley region. Again, our long-term
25 estimate in this region is similar to the ACCMIP and HTAP ensemble means, predicting NO_y
26 deposition in the range of $5\text{--}10 \text{ kg N ha}^{-1} \text{ yr}^{-1}$ (Lamarque et al. 2013; Vet et al. 2014). The
27 elevated deposition here is also spatially consistent with the results from Holland et al. (2005).
28 We find high deposition extending into western Russia with a hotpot in the vicinity of
29 Moscow approaching $5 \text{ kg N ha}^{-1} \text{ yr}^{-1}$. Our observation-constrained estimate also has isolated
30 regions of high deposition in the Middle East (around $4\text{--}5 \text{ kg N ha}^{-1} \text{ yr}^{-1}$ in the vicinity of
31 Tehran and around the Persian Gulf).



1 We find that the highest mean deposition in the world occurs in China, exceeding 10 kg
2 N ha⁻¹ yr⁻¹ in many regions. High deposition extends into the mid-latitude western Pacific
3 Ocean off the coast of East Asia. NO_y deposition in the ACCMIP and HTAP ensemble means
4 also exceeds 10 kg N ha⁻¹ yr⁻¹ throughout eastern China. We find the highest long-term mean
5 deposition (with a maximum close to 20 kg N ha⁻¹ yr⁻¹) occurs in the south, around the Pearl
6 River Delta and in the vicinity of Guangzhou, although deposition is also high in the regions
7 just west of Beijing and Shanghai.

8 In the Southern Hemisphere, high NO_y deposition is associated with biomass burning
9 and soil NO_x sources, in addition to anthropogenic sources. For example, we find NO_y
10 deposition is between 3 to 5 kg N ha⁻¹ yr⁻¹ in central and southern Brazil, and in the tropical
11 rainforests and moist savannahs of Africa. Our estimates in these biomass burning and soil
12 NO_x dominated regions are also generally consistent with the ACCMIP and HTAP ensemble
13 estimates (2-5 kg N ha⁻¹ yr⁻¹). We find NO_y deposition up to 10 kg N ha⁻¹ yr⁻¹ in the vicinity of
14 Sao Paulo and Rio de Janeiro, and in the vicinity of Johannesburg and the industrialized
15 Mpumalanga Highveld of South Africa (all dominated by anthropogenic NO_x emissions). Our
16 constrained simulation also identifies hotspots of deposition in the vicinity of Melbourne and
17 Sydney, Australia (~4 kg N ha⁻¹ yr⁻¹).

18 Figure 1 (bottom) shows the simulated long-term ratio of dry NO_y deposition to total
19 (wet + dry) NO_y deposition. Globally, dry and wet deposition contribute roughly equally to
20 total NO_y deposition (52% and 48% respectively). Dry deposition usually accounts for more
21 than 50% of the total over the continents and directly off shore whereas wet deposition
22 dominates over the remote oceans. In the generally arid regions of the world (e.g.
23 southwestern US, the Sahara Desert, the Arabian Peninsula, and the Gobi Desert) dry
24 deposition accounts for ~85% or more of the total deposition. Elsewhere, dry deposition
25 fractions tend to be highest (>60%) nearest to major surface NO_x sources (e.g. eastern US,
26 Western Europe, and near other major urban centres around the world in addition to the soil
27 and biomass-burning dominated source regions in South America and Africa). HNO₃
28 typically makes the dominant contribution to dry NO_y deposition, although NO₂ and HNO₃
29 can make almost equal contributions in certain high-NO_x environments. Isoprene nitrates and
30 peroxyacetyl nitrates comprise ~10-30% of dry NO_y deposition in some densely forested and
31 high latitude environments respectively.



1 We evaluate our estimates of NO_y deposition with measured wet NO_3^- from several
2 sources. Figure 2 shows measurements of annual wet NO_3^- deposition from the World Data
3 Centre for Precipitation Chemistry, available for two time periods: 2000-2002 ($N = 470$) and
4 2005-2007 ($N = 484$). In both we see the patterns of elevated deposition in eastern North
5 America, Western Europe, and parts of South and East Asia, with lower deposition in western
6 North America, across high latitudes in the Northern Hemisphere, and in the available
7 observations in Africa. High deposition in the Southern Hemisphere is observed between Sao
8 Paulo and Rio de Janeiro, and just southeast of Johannesburg. Figure 2 also shows the wet
9 NO_3^- deposition from our constrained simulation during the same two time periods (2000-
10 2002 and 2005-2007), which exhibits similar patterns found in total NO_y deposition (Figure
11 1).

12 We find a high degree of consistency between our estimate and the observations for
13 both the 2000-2002 ($N = 306$ model-data pairs) and 2005-2007 ($N = 310$ model-data pairs).
14 Normalized mean bias (NMB) is -14% and -16% respectively. The vast majority of pairs (>
15 80%) agree to within 50% of each other. Figure 3 shows scatter plots for specific subsets of
16 the global data. The agreement for both time periods is strongest over North America ($r =$
17 0.92 for both 2000-2002 and 2005-2007, $\text{NMB} = +1.0\%$ and -5.0% respectively). Robust
18 model agreement with wet nitrate deposition observations over densely monitored North
19 America is characteristic of other global studies (Dentener et al. 2006; Lamarque et al. 2013;
20 Vet et al. 2014). Our agreement is also good in Europe ($r = 0.69$ and 0.66 , and $\text{NMB} = -31.0\%$
21 and -29.8% respectively). The weaker correlation and low bias in this region is likewise
22 characteristic of global studies, although our spatial correlation ($r=0.66-0.69$) is on the high
23 end of previously reported multi-model ensembles ($r \sim 0.4-0.6$, Dentener et al. 2006;
24 Lamarque et al. 2013; Vet et al. 2014). The negative bias over Europe compared to North
25 America has previously been attributed to poor modeling of precipitation, and/or spatial
26 representativeness of the measurements compared to model resolution. Throughout the rest of
27 the world (encompassing observations mostly over Asia, but also over eastern Russia, and
28 some locations in the Southern Hemisphere) the combined spatial coverage of the
29 observations is very low ($N = 53$). Normalized mean bias in these estimates is also high
30 compared to North America ($\text{NMB} = -19.5\%$ and -17.8% for 2000-2002 and 2005-2007
31 respectively), and our spatial correlation with the measurements is weak ($r = 0.35$ and 0.42
32 respectively). We find that our poor agreement here is disproportionately driven by the two
33 observations that also have the highest measured deposition in the world: near Port Blair on



1 the South Andaman Island in the Bay of Bengal, and in the Arunachal Pradesh state in
2 northeastern India. Agreement is considerably better with the rest of the data ($r = 0.78$ and
3 0.72 , $NMB = +0.01\%$ and -0.01% for 2000-2002 and 2005-2007 respectively). Excluding
4 these two points substantially improves the global agreement as well (from $r = 0.57$ to 0.75
5 and $r = 0.59$ to 0.75 respectively). Site representativeness, precipitation errors, or uncertainty
6 in our satellite-constrained NO_x emissions may explain the discrepancy at these two specific
7 sites.

8 In addition to global data for 2000-2002 and 2005-2007 from the World Data Centre for
9 Precipitation Chemistry, we also evaluate our estimates of NO_y deposition over the long-term
10 (1996-2014) using continuous observations provided by regional networks. Figure 4 shows
11 measured wet NO_3^- deposition over North America, Europe, and East Asia for locations where
12 at least 15 years of quality-controlled annual data are available. These long-term mean
13 observations demonstrate many of the same spatial patterns as the time slices from 2000-2002
14 and 2005-2007. In North America, a relatively smooth gradient is observed from low
15 deposition in the west to high deposition at sites in the east. In Europe, the highest measured
16 long-term mean wet NO_3^- deposition occurs at a coastal site in southern Norway, at a site just
17 east of Copenhagen, and at locations in northern Italy and in Switzerland. At higher latitude
18 sites, deposition is lower. Across the eastern Asia network, the measurements show highest
19 deposition at sites in Southeast Asia (e.g. at a location between Kuala Lumpur and Singapore,
20 and another in the vicinity of Jakarta) and in Japan. The lowest long-term mean deposition
21 occurs at high latitude sites along the border of Russia and Mongolia, while moderate to high
22 deposition is measured on the coast of eastern China.

23 In general, our satellite-constrained estimate reflects the spatial variability that is seen in
24 the measurements. Globally, the correlation between measured NO_3^- deposition and our
25 estimated wet NO_3^- deposition is excellent ($r = 0.83$, $NMB = -7.7\%$, $N = 136$ gridded model-
26 data pairs). The vast majority of pairs ($> 85\%$) agree to within 50% of each other. For the
27 individual regions, normalized mean bias in our estimate is smallest over North America
28 ($NMB = +2.4\%$), and higher over Europe and East Asia ($NMB = -32\%$ and -25%
29 respectively). The spatial correlation over each region is strong ($r = 0.89$, $r = 0.87$, and $r =$
30 0.69 for North America, Europe, and East Asia respectively), but sample sizes over Europe (N
31 $= 16$) and East Asia ($N = 11$) are small so we emphasize caution in the interpretation of the
32 statistics for these two regions. The lack of continuous measurement coverage even in parts of



1 the world with routine network observations highlights the imperative of using other novel
2 observational constraints on deposition (such as the global satellite observations of NO₂ used
3 here).

4 **3.2 Trends in Global NO_y Deposition from 1996 to 2014**

5 Our long-term satellite-constrained estimate of NO_y deposition facilitates a unique and
6 up-to-date investigation of the changes in NO_y deposition around the world. We calculate
7 linear trends in annual NO_y deposition using the nonparametric Sen's method (Sen, 1968),
8 and test for significance with the nonparametric Mann-Kendall method (Kendall, 1975;
9 Mann, 1945). We treat increasing or decreasing trends as significant if $p < 0.01$. Given that
10 this is a test for linear trends, regions where shorter-term trends in deposition may have
11 changed signs over the period of study could result in erroneous or insignificant trends. Below
12 we discuss particular regions where this is the case.

13 Figure 5 shows the long-term annual and seasonal trends calculated from our satellite-
14 constrained estimate of total NO_y deposition across 1996-2014 (hatching indicates statistical
15 significance). Figure 6 highlights timeseries of total NO_y deposition over three specific
16 regions covering parts of North America, Western Europe, and East Asia (as outlined in
17 dashed boxes in the top panel of Fig. 5).

18 Substantial decreases are seen throughout North America extending over the Atlantic
19 Ocean to remote regions. The timeseries for this region (Fig. 6, left) shows that NO_y
20 deposition decreased by almost 40% from 6.4 Tg N yr⁻¹ in 1996-1998 to 3.9 Tg N yr⁻¹ in
21 2012-2014. The steepest local decline in the world appears over the Ohio River Valley area,
22 with a maximum near Pittsburgh where NO_y deposition decreased by -0.6 kg N ha⁻¹ yr⁻². NO_y
23 deposition near Pittsburgh decreased from consistently exceeding 15 kg N ha⁻¹ yr⁻¹ during
24 1996-2000, to below 6 kg N ha⁻¹ yr⁻¹ by 2014. The strong decrease in the northeast is
25 consistent with other long-term observational studies for the US (Sickles II and Shadwick,
26 2007, 2015). Studies of US NO_x emissions derived from satellite observations have also
27 highlighted the remarkable success of emission controls (Duncan et al., 2013; Russell et al.,
28 2012). Our constrained estimate has the steepest declines during the summer (Fig 5, JJA),
29 restricted tightly to the source regions. This also agrees with long-term observations showing
30 the strongest reductions in the summer (Sickles II and Shadwick 2015), consistent with the
31 shorter lifetime of NO_x and efficient dry deposition of NO_y over the forested eastern US. We



1 find significant decreases far downwind over the Atlantic Ocean during the other months,
2 when NO_y can be transported farther. The steep change in NO_y deposition in the eastern US
3 over the last 20 years may have important consequences on tree mortality rates in the region,
4 which have been demonstrated to be very sensitive to NO_3^- deposition in the range of 5-15 kg
5 $\text{N ha}^{-1} \text{ yr}^{-1}$ (Dietze and Moorcroft, 2011). The steeply decreasing trends across the US in our
6 satellite-derived NO_y also support the increasing dominance of reduced nitrogen in total
7 nitrogen deposition evidenced by observations (Li et al., 2016) and model predictions (Ellis et
8 al., 2013).

9 We find a small but statistically significant positive trend in NO_y deposition (+0.06 kg
10 $\text{N ha}^{-1} \text{ yr}^{-2}$) in northern Alberta, Canada, dominated by the trend in JJA. The region is
11 downwind of development in the Canadian oil sands, which has seen notable changes in NO_2
12 column abundance as observed from space (McLinden et al., 2012). We estimate that
13 deposition of NO_y in this area was at a maximum of 3.4 kg $\text{N ha}^{-1} \text{ yr}^{-1}$ in 2011 (up from 1.3 kg
14 $\text{N ha}^{-1} \text{ yr}^{-1}$ in 1996-1997), and has since declined to 1.6 kg $\text{N ha}^{-1} \text{ yr}^{-1}$ by 2014. Elsewhere in
15 Canada we estimate that NO_y deposition has decreased in the south and east parts of the
16 country, consistent with observational analyses (Zbieranowski and Aherne, 2011).

17 Declines in NO_y deposition are also found across Europe, but statistical significance
18 tends to be limited to western continental Europe and the United Kingdom (while changes in
19 the south, north, and eastern countries tend to be insignificant). According to the timeseries
20 for this region (Fig. 6, middle), NO_y deposition decreased by about 15% (from 2.5 Tg N yr^{-1}
21 in 1996-1998 to 2.1 Tg N yr^{-1} in 2012-2014). We find the steepest local trends (-0.1 kg N ha^{-2}
22 yr^{-1}) in eastern Germany and southern UK, where NO_y deposition in 2012-2014 decreased by
23 20% compared to 1996-1998. Previous satellite constraints on NO_x emissions established that
24 NO_x emissions in France, Germany, Great Britain, and Poland have declined since 1996 while
25 emissions in Greece, Italy, Spain, and the Ukraine for example have either stayed constant or
26 increased (Konovalov et al., 2008). The local variability in emission trends leads to notable
27 transboundary impacts. For example, our simulation predicts no net trend in NO_y deposition
28 over the Ukraine; but we find this is a result of opposing trends in dry (increasing) and wet
29 (decreasing) deposition. This would be explained by increasing local emissions but decreasing
30 transport from upwind. Similarly, we find significant increases in dry deposition in parts of
31 western Russia but no significant trend in wet deposition.



1 Large increases in NO_y deposition are found throughout Asia, concentrated especially in
2 eastern China and parts of Southeast Asia. Figure 6 shows the timeseries of wet and dry NO_y
3 deposition within the rectangular region outlined in Figure 5 that encompasses eastern China
4 and part of the adjacent ocean. We find that NO_y deposition in the region increased by 65%
5 from 5.2 Tg N yr^{-1} in 1996-1998 to 8.6 Tg N yr^{-1} in 2012-2014. The timeseries also shows
6 that NO_y deposition decreased after peaking around 9.3 Tg N yr^{-1} in 2011-2012. We find that
7 the steepest increasing local trends in the world appear in eastern China, and in the Pearl
8 River Delta region (up to $+0.6 \text{ kg N ha}^{-1} \text{ yr}^{-2}$). In fact, deposition in the Pearl River Delta
9 region is the highest in the world for most of our record, exceeding $20 \text{ kg N ha}^{-1} \text{ yr}^{-1}$ every
10 year from 2003-2014 (almost doubling from just over $11 \text{ kg N ha}^{-1} \text{ yr}^{-1}$ in 1996). The trends in
11 deposition over China are largest in summer when the NO_x lifetime is short, with more
12 obvious indications of increasing NO_y transport/export in the spring months (Fig 5, MAM).
13 The substantial increase in NO_x emissions throughout East Asia has been inferred from
14 satellite instruments in several previous studies (Mijling et al., 2013; Richter et al., 2005).
15 The timing and extent of the reversal in NO_y deposition that we see is also consistent with
16 observed NO_2 columns over eastern China derived from OMI (de Foy et al., 2016; Krotkov et
17 al., 2016). The ability of our satellite-constrained NO_y deposition estimate to capture this
18 sudden dramatic decrease over China, in contrast with previous projections (e.g. the RCP2.6,
19 RCP4.5, and RCP8.5 projections to 2030, Lamaque et al. 2013), emphasizes an attribute of
20 the satellite constraint.

21 Small statistically significant decreasing trends are found over the biomass-burning
22 dominated source regions of Africa. The decrease in NO_y deposition of about $\sim 3\% \text{ yr}^{-1}$
23 relative to the long-term mean in Northern Africa is consistent with the most recent GFED4
24 inventory from 1997 to 2014 (<http://www.globalfiredata.org/>), which has fire NO_x emissions
25 decreasing at a rate of about $3\% \text{ yr}^{-1}$ in this region. In contrast, we also estimate a similar
26 decrease in Southern Africa that is not represented in the recent GFED4 emission timeseries.
27 A reduction in NO_2 column abundance in this region (observed by GOME and
28 SCIAMACHY) was also reported by van der A. (2008). They postulate that this decline could
29 be a result of deforestation leading to less biomass burning, but changing NO_x emission
30 factors from biomass burning could also potentially explain the trend.

31 Despite the large regional trends described above, we find that global deposition
32 changed very little between 1996-1998 ($56.1 \text{ Tg N yr}^{-1}$) and 2012-2014 ($58.5 \text{ Tg N yr}^{-1}$) due



1 to the opposing changes in different regions. Total NO_y deposition was lowest in 2006 (50.5
2 Tg N), and peaked at 60.8 Tg N in 2012. Since then, it appears that global NO_y deposition
3 may be on the decline. Future observations in the coming years will be needed to establish
4 whether this most recent decline is robust or temporary.

5 Figure 7 shows the calculated long-term trends in the measured wet NO_3^- deposition for
6 locations across North America, Europe, and East Asia where at least 15 years of quality-
7 controlled annual data are available (the coverage of these observation is the same as in
8 Figure 4). The observations over North America show the gradient in trend from negligible in
9 the west to steeply and significantly decreasing in northeastern US and southeastern Canada.
10 The steepest observed statistically significant trend ($-0.18 \text{ kg N ha}^{-1} \text{ yr}^{-2}$) occurs east of
11 Detroit in southwestern Ontario, Canada. In Europe, only one of the gridded observations has
12 a statistically significant trend ($-0.07 \text{ kg N ha}^{-1} \text{ yr}^{-2}$), located near the border of Denmark and
13 Germany. The other locations in Europe show statistically insignificant trends over the long-
14 term. In East Asia, we also we find that most of the stations record statistically negligible
15 trends over the long term (only two of the 11 gridded observations have significant trends).
16 The steepest observed trend in this region ($+0.39 \text{ kg N ha}^{-1} \text{ yr}^{-2}$) is found near Kuala Lumpur
17 and is statistically significant.

18 We compare the long-term trends in these measurements with our satellite-constrained
19 trends in wet NO_3^- deposition. We find a similar spatial gradient in North America, and the
20 same magnitude of declines through the northeast US and southern Ontario (-0.12 to -0.16 kg
21 $\text{N ha}^{-1} \text{ yr}^{-2}$). Over Europe, our estimates have low statistical significance in the trends
22 throughout much of this region, consistent with the observations. Where we do see statistical
23 significance (northern United Kingdom, southern Denmark, and in some central/eastern
24 European countries), observations are not available over the long-term for evaluation. In East
25 Asia, our satellite-constrained estimated trends show statistically significant increases
26 throughout much of the region (in contrast to most of the available observations). The trend
27 over Kuala Lumpur is significant and positive ($+0.24 \text{ kg N ha}^{-1} \text{ yr}^{-2}$) as expected from the
28 available measurements.

29 We again emphasize the small sample size in Europe ($N = 16$) and East Asia ($N = 11$).
30 Moreover, in many cases trends in one (or both) datasets are small and/or insignificant. For
31 these reasons, we focus on comparing the confidence intervals of the measured and satellite-
32 constrained trends. We find that for 129 of the 136 gridded pairs ($> 90\%$ of the data), the 95%



1 confidence intervals overlap; of the pairs for which the intervals do not overlap, 3 (out of 109)
2 occur in North America, 1 (out of 16) in Europe, and 3 (out of 11) in East Asia. For a large
3 majority of the data in all three regions we therefore conclude that the satellite-derived trends
4 are not significantly different from the trends inferred with ground-based measurements.
5 Continued long-term measurements with better spatial coverage are imperative to better
6 evaluate long-term estimates of global NO_y deposition especially throughout Europe and East
7 Asia (but also in other parts of the world where long-term coverage is not available at all).

8 **3.3 Changes in Continental Export of NO_y**

9 NO_y deposition is a transboundary, and even intercontinental, issue (HTAP, 2010). In a
10 multi-model study, Sanderson et al. (2008) found that between 3-10% of NO_x emissions from
11 Europe, North America, South Asia, and East Asia are ultimately deposited over foreign
12 regions. Long range transport events of NO_2 alone can be systematically detected by satellite
13 observations (Zien et al., 2014). Here we extend such studies using our satellite-constrained
14 long-term estimates of annual NO_y deposition to evaluate how the amount of NO_x exported
15 from specific regions (i.e. the net balance between emissions and deposition over a land area)
16 has changed over the last two decades.

17 Decreases in NO_y export over the Atlantic Ocean from North America and increases in
18 export over the western Pacific Ocean from East Asia are evident in Figure 5. We find that net
19 export of NO_x from North America via atmospheric transport has decreased by more than
20 40% (from 2.5 Tg N yr^{-1} in 1996, to 1.4 Tg N yr^{-1} in 2014). In contrast, we find that export of
21 NO_x from Asia increased by 40% from 3.3 Tg N in 1996, to a maximum of 4.7 Tg N in 2011,
22 with a subsequent decrease to 3.8 Tg N by 2014. As a result of these opposing trends, total
23 deposition to the global oceans has changed remarkably little (25.0 Tg N yr^{-1} in 1996-1998
24 compared to 24.4 Tg N yr^{-1} in 2012-2014), but has experienced substantial regional
25 redistribution.

26 NO_y export from North America has received considerable attention. Urban plumes
27 from the eastern US that are transported across the North Atlantic for several days could still
28 contain 20-50 ppb of reactive nitrogen oxides (Neuman et al. 2006). A recent detailed GEOS-
29 Chem study of nitrogen deposition over the US estimated that net annual export of NO_x was
30 around 38% of NO_x emissions (or 2.5 Tg N) for 2006-2008 (Zhang et al. 2012). We estimate
31 a similar fraction of export from the continental US using our observationally-constrained



1 simulation ($34\% \pm 2\%$ from 1996-2014). As a result of declining emissions we find that
2 absolute export from the continental US decreased by 50% from 2.9 Tg N in 1996 to 1.5 Tg N
3 in 2014. We find declines in NO_y deposition across the Atlantic Ocean, with small though
4 statistically significant declines as far downwind as southern Greenland. The decreases
5 downwind of the continent are clearest and most significant in the winter, spring, and fall
6 (Fig. 5b, c, and e) while the trends are more local in the summer (when the NO_x lifetime is
7 short and when midlatitude wind speeds are weaker.

8 We similarly calculate the net imbalance between NO_x emissions and NO_y deposition
9 over western European countries and find a decrease of almost 40%, from 2.2 Tg N to 1.3 Tg
10 N. In contrast to the continental US, we also find a notable decrease in the fraction of
11 emissions that are exported from western European countries (from 50% in 1996-1998 to
12 40% in 2012-2014). As a result, the decrease in net export is steeper than the decrease in
13 emissions from the region. As alluded to in Section 3.2, the decrease in NO_x export from
14 some western European countries has likely compensated for increases in emissions in some
15 of the central/eastern European countries, and in western Russia, where we find dry
16 deposition has significantly increased, but wet deposition has decreased or shows no
17 significant net trend.

18 Reactive nitrogen transport from Asia has previously been shown to contribute to O_x
19 production across the mid-latitude Pacific reaching as far as the west coast of North America
20 (Walker et al., 2010; Zhang et al., 2008), and major NO_x transport events from China can be
21 indirectly observed by NO_2 columns (Lee et al., 2014). Our satellite-constrained estimate
22 predicts that export from China alone ($24\% \pm 4\%$ of emissions) more than tripled from 1.0 Tg
23 N in 1996 to a maximum of 3.5 Tg N in 2011, then decreased to 2.5 Tg N by 2014. Zhao et al.
24 (2015) used GEOS-Chem to explore nitrogen deposition to the northwestern Pacific Ocean
25 off the coast of China from 2008-2010. They estimated total (wet + dry) NO_y deposition of
26 $6.9 \text{ kg N ha}^{-1} \text{ yr}^{-1}$ and $3.1 \text{ kg N ha}^{-1} \text{ yr}^{-1}$ to the Yellow Sea and the South China Sea
27 respectively. Our simulation predicts that NO_y deposition to the same regions of the Yellow
28 Sea increased from $5.1 \text{ kg N ha}^{-1} \text{ yr}^{-1}$ in 1996 to $9.5 \text{ kg N ha}^{-1} \text{ yr}^{-1}$ by 2012 and to the South
29 China Sea from $2.8 \text{ kg N ha}^{-1} \text{ yr}^{-1}$ in 1996 to $4.3 \text{ kg N ha}^{-1} \text{ yr}^{-1}$ in 2011. Subsequent declines in
30 the following years will hopefully have encouraging implications for nitrogen availability and
31 the incidence of algal blooms in these regions (Hu et al., 2010).



1 Export of pollution from China has been shown to influence deposition over Japan in
2 particular (e.g. Lin et al., 2008). Using observations of wet nitrate deposition, Morino et al.
3 (2011) report increases throughout Japan from 1989-2008, and attribute this trend largely to
4 transport from China. Likewise, integrated NO_y deposition over Japan increased ($p < 0.01$) in
5 our satellite-constrained estimate. In fact, we find that Japan transitioned from a net
6 “exporter” of NO_y over 1996-2006 (emissions exceeded local deposition by up to 24%) to a
7 net “importer” of NO_y over 2007-2014 (local deposition exceeded emissions by up to 20%).
8 The increase in deposition was dominated by statistically significant increases in wet
9 deposition in some parts of the country. We find the increase over Japan is most uniform
10 during the spring (Fig. 5, MAM), consistent with transport from China being pronounced
11 during the spring season (Tanimoto et al., 2005). Nevertheless, the impacts of local NO_x
12 controls can also be important. Dry deposition dominates the decline in annual NO_y
13 deposition just west of Tokyo. Declines are seen throughout the southern part of the country
14 during both the summer and fall seasons (Fig. 5, JJA and SON). These results demonstrate the
15 indirect relationship between local emissions and local deposition of NO_y for regions
16 influenced by atmospheric transport, and also show how long-term trends can depend strongly
17 on the season and process (wet or dry deposition).

18 **3.4 Sensitivity of NO_y Deposition to NH_3 Emissions**

19 The transport and ultimate deposition of oxidized nitrogen may be tightly coupled with
20 the reduced nitrogen ($\text{NH}_x = \text{NH}_3 + \text{NH}_4^+$) and sulfate systems, due to the formation of
21 NH_4NO_3 aerosol that becomes favorable once all H_2SO_4 has been neutralized (i.e., if there is
22 “excess” NH_3). Examples of the resulting non-linearity between $\text{PM}_{2.5}$ concentrations and
23 precursor emissions have been noted in the literature (Banzhaf et al., 2013; Derwent et al.,
24 2009; Fowler et al., 2005). The formation of NH_4NO_3 aerosol at the expense of HNO_3 with
25 changing excess ammonia could therefore conceivably change the atmospheric lifetime of
26 NO_y at the surface; accumulation mode aerosol may have a dry deposition lifetime of days
27 whereas HNO_3 tends to have a dry deposition lifetime of shorter than a day. As a result, the
28 predicted footprint of source impacts is sensitive to NH_3 emissions (Lee et al., 2016).

29 Contemporary emissions of NH_3 are highly uncertain (Reis et al., 2009), so we perform
30 a sensitivity experiment by perturbing NH_3 emissions everywhere by 25% for the year 2012.
31 Predicted NO_y deposition from this simulation is compared to the predicted NO_y deposition in
32 the 2012 simulation where NH_3 emissions were not perturbed. Since we have not altered the



1 emissions of oxidized nitrogen, simple mass balance dictates that increases in deposition over
2 some regions will be countered by decreases elsewhere. Our perturbation is therefore to be
3 interpreted as an experiment that tests how accurately the spatial pattern in NO_y deposition at
4 our model resolution can be predicted, given some uncertainty in NH_3 emissions. Given the
5 horizontal resolution of our simulation ($2.5^\circ \times 2.0^\circ$), we acknowledge that our estimates of the
6 sensitivity of NO_y deposition to perturbations in NH_3 emissions may underestimate the
7 importance of those interactions at finer spatial scales.

8 Figure 8 shows the results of this experiment. The sensitivity of NO_y deposition to an
9 increase in NH_3 emissions is positive or negative depending on the region, while net
10 deposition over the global domain does not change (to within 1-2%). Over the continents, the
11 sensitivity in total (wet + dry) NO_y deposition to the 25% perturbation in NH_3 emissions tends
12 to be less than $\pm 5\%$, with a few exceptions. We find differences in NO_y deposition on the
13 order of 10% over parts of high-latitude Russia, northwest and central Africa, eastern China,
14 southern South America, and Australia. However, with the exception of China, these are also
15 regions where deposition is relatively low. We conclude that for most regions of interest, our
16 satellite-constrained estimates of NO_y deposition over the continents and their trends will not
17 be severely impacted by uncertainty in the NH_3 inventories.

18 Notably, the difference exceeds +50% over Myanmar, suggesting that simulated NO_y
19 deposition over this country is extremely sensitive to changes in NH_3 emissions. It is clear
20 from Figure 8 that this results from a high sensitivity in dry deposition (middle panel) instead
21 of wet deposition (bottom panel). Myanmar has some of the lowest estimated NH_3 emissions
22 in all of South and East Asia (at least an order of magnitude lower than surrounding India,
23 China, and Thailand), so this sensitivity reflects changes in the upwind emissions and
24 subsequent transport of NO_y . We find the opposite sensitivity in nearby Cambodia, where the
25 sensitivity of dry NO_y deposition to a 25% perturbation in NH_3 emissions is -50%.

26 Over the oceans, the sensitivity of NO_y deposition to the 25% increase in NH_3 emissions
27 is generally low ($< \pm 5\%$), with the expected exceptions in areas that are directly offshore
28 from major continental source regions. In the North Atlantic Ocean east of Canada and
29 Greenland, and in the North Pacific Ocean off the coasts of China, Japan and in the South
30 China Sea, the sensitivity of NO_y deposition is between 5-20%. Our predicted decrease in dry
31 NO_y deposition to the Yellow Sea given an increase in NH_3 emissions is consistent with
32 previous adjoint analyses showing increased NO_y dry deposition in this region with a decrease



1 in Asian NH_3 emissions (Zhao et al. 2015). Likewise, the sensitivity of deposition to the
2 Mediterranean Sea is between 10-20%. The differences in NO_y deposition over the oceans
3 results from sensitivity in both dry and wet deposition (although in the case of the
4 Mediterranean it is dominated by dry deposition). We conclude that although changes (or
5 uncertainties) in NH_3 emissions can impact the distance of transport and deposition to oceans
6 downwind of the major NO_x sources, the absolute magnitude of deposition is low where the
7 sensitivity of NO_y deposition to NH_3 is relatively high.

8

9 **4 Conclusion**

10 NO_y deposition represents about half of the total reactive nitrogen deposited to Earth's
11 surface. Even in the US where nitrogen oxide emissions have decreased substantially,
12 constituents of NO_y remain major contributors to the nitrogen deposited in areas of concern
13 (Lee et al. 2016; Li et al. 2016). We applied NO_2 observations from multiple satellites over
14 1996-2014 together with the GEOS-Chem chemical transport model to estimate long-term
15 changes to reactive nitrogen oxide deposition around the world. Given the effective global
16 mass balance between NO_x emissions and deposition of reactive nitrogen oxides, we show
17 that satellite constraints on NO_x emissions can provide a powerful top-down constraint on
18 deposition in order to evaluate long-term changes worldwide. Observations from the GOME,
19 SCIAMACHY, and GOME-2 satellite instruments have provided continuous global coverage
20 over the last 20 years, allowing observational constraints on NO_y deposition that enhance the
21 poor spatial coverage of ground-based deposition measurements.

22 We find substantial variability in regional trends of NO_y deposition. NO_y deposition
23 declined most steeply throughout the northeastern United States by up to $-0.6 \text{ kg N ha}^{-1} \text{ yr}^{-2}$,
24 but has also decreased significantly throughout most of the country and in southern Canada.
25 In Europe, statistically significant declines of up to $-0.1 \text{ kg N ha}^{-1} \text{ yr}^{-2}$ are seen over some
26 western countries. On the other hand, NO_y deposition has increased substantially throughout
27 East Asia, exceeding $+0.6 \text{ kg N ha}^{-1} \text{ yr}^{-2}$ in some parts. Since reductions in deposition over
28 some regions were counteracted by increases in others, global NO_y deposition did not change
29 considerably over the long term. However, we find that global NO_y deposition could now be
30 on the decline overall, since deposition in Asia peaked around 2010-2012. The ability to
31 resolve the striking recent decline in NO_y deposition in China (despite prior projections of



1 increasing NO_x emissions) demonstrates one of the attributes of using a satellite-based
2 constraint. Future observations will be important in evaluating whether this trend persists.

3 We find that changes over the last two decades in the export of reactive nitrogen oxides
4 via atmospheric transport have impacted countries downwind of source regions. Export from
5 North America has decreased by at least 40%, while export from Asia has increased by the
6 same relative amount. We find evidence that decreases in NO_x export from some western
7 European countries have counteracted increases in local emissions from some eastern/central
8 European countries, resulting in negligible net change in NO_y deposition over the long term.
9 Likewise, Japan is highly sensitive to changes in export from China, but this depends strongly
10 on the season and whether wet and dry deposition are both considered. While uncertainty in
11 NH_3 emissions can impact the footprint of NO_y export and deposition, we show that this
12 sensitivity is small in most regions of concern.

13 Direct measurements of deposition are sparse, inhibiting evaluation. This is especially
14 challenging for global simulations, where individual measurements may not necessarily be
15 regionally representative. Nevertheless, we find that for the vast majority of locations our
16 satellite-derived trends are largely consistent with the observed trends. Expanded coverage of
17 ground-based observations over the long-term is needed to more comprehensively evaluate
18 long-term estimates of global NO_y deposition. This need also motivates the value of using
19 alternative observational constraints like the satellite NO_2 columns as presented here.

20 Forthcoming satellite observations of NO_2 at higher spatial resolution (e.g. TROPOMI
21 (Veeffkind et al., 2012)) and with diurnally varying observations (e.g. TEMPO (Zoogman et
22 al., 2016), Sentinel-4, and GEMS) will offer increasingly robust constraints on NO_x emissions
23 that affect NO_y deposition. Satellite observations of NH_3 (e.g. Van Damme et al., 2014) may
24 offer additional opportunities to constrain the reactive nitrogen budget. Higher resolution
25 global modeling will also be an important development to accurately account for non-linear
26 NO_2 losses in global emission inversions (Valin et al., 2011).

27 Our satellite-constrained estimates of NO_y document interannual changes over the past
28 two decades worldwide. We expect that this information will be useful in future research into
29 the impacts of nitrogen deposition to important biodiversity hotspots, in regions dealing with
30 excessive nitrogen inputs leading to algal blooms, or estimating the changing impacts of
31 nitrogen deposition on global carbon uptake.

32



1 Appendix 1

2 We simulate atmospheric chemistry from 1996 to 2014 using the GEOS-Chem
3 chemical transport model (www.geos-chem.org) v9-02. Our simulations are driven with the
4 MERRA meteorological product at a global horizontal resolution of $2.5^\circ \times 2.0^\circ$ and 47
5 vertical layers. GEOS-Chem includes detailed HO_x - NO_x -VOC- O_3 -aerosol chemistry (Bey et
6 al. 2001; Park et al. 2004), with isoprene chemistry following Paulot et al. (2009a, 2009b) and
7 gas-aerosol partitioning for the sulfate-nitrate-ammonium system calculated according to the
8 ISORROPIA II equilibrium model (Fountoukis and Nenes, 2007). Gas-aerosol phase coupling
9 occurs via N_2O_5 uptake (Evans and Jacob, 2005) and HO_2 uptake (Mao et al., 2013) in
10 addition to other heterogeneous chemistry (Jacob, 2000) and aerosol effects on photolysis
11 frequencies (Martin et al., 2003). Our simulations use timesteps of 15 minutes for transport
12 and convection, and 30 minutes for emissions and chemistry.

13 Removal by wet deposition occurs through scavenging in moist convective updrafts, as
14 well as in-cloud and below-cloud scavenging during large-scale precipitation for water-
15 soluble aerosol and gases (Amos et al., 2012; Liu et al., 2001). Removal by dry deposition is
16 calculated based on the widely used resistance-in-series formulation from Wesely (1989),
17 described for GEOS-Chem in Wang et al. (1998) and Zhang et al. (2001) for aerosol. Dry
18 deposition of NO_y over the United States was recently explored and evaluated in detail by
19 Zhang et al. (2012).

20 Anthropogenic emissions are prescribed by the NEI 2005 inventory for the United
21 States (<http://www.epa.gov/ttnchie1/trends/>), the CAC inventory for Canada
22 (<http://www.ec.gc.ca/pdb/cac/>), the BRAVO inventory for Mexico (Kuhns et al., 2005), the
23 EMEP inventory for Europe (<http://www.emep.int/>), and Zhang et al. (2009) for China and
24 Southeast Asia. Elsewhere, the EDGAR v3 emission inventory is used for anthropogenic
25 NO_x , CO, and SO_x (Olivier et al., 2005), the GEIA inventory for NH_3 (Bouwman et al., 1997),
26 and the RETRO inventory for VOCs (Hu et al., 2015). Aircraft emissions are from the AEIC
27 inventory (Stettler et al., 2011). Scale factors based on energy statistics following van
28 Donkelaar et al. (2008) are used to scale NO_x , CO and SO_x emissions between 1996 and 2010
29 for years when the emissions are unavailable from the inventory. For other species and for
30 emissions beyond 2010, the closest available year is used. Biogenic VOC emissions are
31 calculated using the MEGAN model (Guenther et al., 2006). Biomass burning emissions are
32 according to the GFED3 inventory (Mu et al., 2011). Soil NO_x is calculated using the



1 Berkeley-Dalhousie Parameterization (Hudman et al., 2012). Lightning NO_x is implemented
2 according to Murray et al. (2012). These a-priori surface NO_x emissions are overwritten by
3 our satellite-derived top-down estimates in the assessment of NO_y deposition.

4

5

6 **Acknowledgements**

7 This work was supported by NSERC and Environment and Climate Change Canada. We
8 acknowledge the free use of tropospheric NO₂ column data from the GOME, SCIAMACHY,
9 and GOME-2 sensors from www.temis.nl. We further acknowledge the NADP, CAPMoN,
10 EMEP and EANET regional monitoring networks, and the World Data Centre for
11 Precipitation Chemistry for access to wet deposition data.

12



1 **References**

- 2 van der A, R. J., Eskes, H. J., Boersma, K. F., van Noije, T. P. C., Van Roozendaal, M., De
3 Smedt, I., Peters, D. H. M. U. and Meijer, E. W.: Trends, seasonal variability and dominant
4 NO_x source derived from a ten year record of NO₂ measured from space, *J. Geophys. Res.*,
5 113(D4), D04302, doi:10.1029/2007JD009021, 2008.
- 6 Amos, H. M., Jacob, D. J., Holmes, C. D., Fisher, J. A., Wang, Q., Yantosca, R. M., Corbitt,
7 E. S., Galarnau, E., Rutter, A. P., Gustin, M. S., Steffen, A., Schauer, J. J., Graydon, J. A.,
8 Louis, V. L. St., Talbot, R. W., Edgerton, E. S., Zhang, Y. and Sunderland, E. M.: Gas-
9 particle partitioning of atmospheric Hg(II) and its effect on global mercury deposition, *Atmos.*
10 *Chem. Phys.*, 12(1), 591–603, doi:10.5194/acp-12-591-2012, 2012.
- 11 Banzhaf, S., Schaap, M., Wichink Kruit, R. J., Denier van der Gon, H. A. C., Stern, R. and
12 Builtjes, P. J. H.: Impact of emission changes on secondary inorganic aerosol episodes across
13 Germany, *Atmos. Chem. Phys.*, 13(23), 11675–11693, doi:10.5194/acp-13-11675-2013,
14 2013.
- 15 Beirle, S., Huntrieser, H. and Wagner, T.: Direct satellite observation of lightning-produced
16 NO_x, *Atmos. Chem. Phys.*, 10(22), 10965–10986, doi:10.5194/acp-10-10965-2010, 2010.
- 17 Bey, I., Jacob, D. J., Yantosca, R. M., Logan, J. A., Field, B. D., Fiore, A. M., Li, Q., Liu, H.
18 Y., Mickley, L. J. and Schultz, M. G.: Global modeling of tropospheric chemistry with
19 assimilated meteorology: Model description and evaluation, *J. Geophys. Res.*, 106(D19),
20 23073, doi:10.1029/2001JD000807, 2001.
- 21 Bobbink, R., Hicks, K., Galloway, J., Spranger, T., Alkemade, R., Ashmore, M., Bustamante,
22 M., Cinderby, S., Davidson, E., Dentener, F., Emmett, B., Erisman, J.-W., Fenn, M., Gilliam,
23 F., Nordin, A., Pardo, L. and De Vries, W.: Global assessment of nitrogen deposition effects
24 on terrestrial plant diversity: a synthesis, *Ecol. Appl.*, 20(1), 30–59, doi:10.1890/08-1140.1,
25 2010.
- 26 Boersma, K. F., Eskes, H. J. and Brinksma, E. J.: Error analysis for tropospheric NO₂
27 retrieval from space, *J. Geophys. Res.*, 109(D4), D04311–D04311,
28 doi:10.1029/2003JD003962, 2004.
- 29 Boersma, K. F., Vinken, G. C. M. and Eskes, H. J.: Representativeness errors in comparing
30 chemistry transport and chemistry climate models with satellite UV–Vis tropospheric column



- 1 retrievals, *Geosci. Model Dev.*, 9(2), 875–898, doi:10.5194/gmd-9-875-2016, 2016.
- 2 Bouwman, A. F., Lee, D. S., Asman, W. A. H., Dentener, F. J., Van Der Hoek, K. W. and
3 Olivier, J. G. J.: A global high-resolution emission inventory for ammonia, *Global*
4 *Biogeochem. Cycles*, 11(4), 561–587, doi:10.1029/97GB02266, 1997.
- 5 Bouwman, A. F., Van Vuuren, D. P., Derwent, R. G. and Posch, M.: A Global Analysis of
6 Acidification and Eutrophication of Terrestrial Ecosystems, *Water. Air. Soil Pollut.*, 141(1/4),
7 349–382, doi:10.1023/A:1021398008726, 2002.
- 8 Castellanos, P. and Boersma, K. F.: Reductions in nitrogen oxides over Europe driven by
9 environmental policy and economic recession., *Sci. Rep.*, 2, 265, doi:10.1038/srep00265,
10 2012.
- 11 Cheng, M., Jiang, H., Guo, Z., Zhang, X. and Lu, X.: Estimating NO₂ dry deposition using
12 satellite data in eastern China, *Int. J. Remote Sens.*, 34(7), 2548–2565,
13 doi:10.1080/01431161.2012.747019, 2013.
- 14 Van Damme, M., Clarisse, L., Heald, C. L., Hurtmans, D., Ngadi, Y., Clerbaux, C., Dolman,
15 A. J., Erisman, J. W. and Coheur, P. F.: Global distributions, time series and error
16 characterization of atmospheric ammonia (NH₃) from IASI satellite observations, *Atmos.*
17 *Chem. Phys.*, 14(6), 2905–2922, doi:10.5194/ACP-14-2905-2014, 2014.
- 18 Dentener, F., Drevet, J., Lamarque, J. F., Bey, I., Eickhout, B., Fiore, A. M., Hauglustaine, D.,
19 Horowitz, L. W., Krol, M., Kulshrestha, U. C., Lawrence, M., Galy-Lacaux, C., Rast, S.,
20 Shindell, D., Stevenson, D., Van Noije, T., Atherton, C., Bell, N., Bergman, D., Butler, T.,
21 Cofala, J., Collins, B., Doherty, R., Ellingsen, K., Galloway, J., Gauss, M., Montanaro, V.,
22 Müller, J. F., Pitari, G., Rodriguez, J., Sanderson, M., Solmon, F., Strahan, S., Schultz, M.,
23 Sudo, K., Szopa, S. and Wild, O.: Nitrogen and sulfur deposition on regional and global
24 scales: A multimodel evaluation, *Global Biogeochem. Cycles*, 20(4), n/a-n/a,
25 doi:10.1029/2005GB002672, 2006.
- 26 Derwent, R., Witham, C., Redington, A., Jenkin, M., Stedman, J., Yardley, R. and Hayman,
27 G.: Particulate matter at a rural location in southern England during 2006: Model sensitivities
28 to precursor emissions, *Atmos. Environ.*, 43(3), 689–696,
29 doi:10.1016/j.atmosenv.2008.09.077, 2009.
- 30 Dietze, M. C. and Moorcroft, P. R.: Tree mortality in the eastern and central United States:
31 patterns and drivers, *Glob. Chang. Biol.*, 17(11), 3312–3326, doi:10.1111/j.1365-



- 1 2486.2011.02477.x, 2011.
- 2 van Donkelaar, A., Martin, R. V., Leaitch, W. R., Macdonald, A. M., Walker, T. W., Streets,
3 D. G., Zhang, Q., Dunlea, E. J., Jimenez, J. L., Dibb, J. E., Huey, L. G., Weber, R. and
4 Andreae, M. O.: Analysis of aircraft and satellite measurements from the Intercontinental
5 Chemical Transport Experiment (INTEX-B) to quantify long-range transport of East Asian
6 sulfur to Canada, *Atmos. Chem. Phys.*, 8(11), 2999–3014, doi:10.5194/acp-8-2999-2008,
7 2008.
- 8 Duce, R. A., LaRoche, J., Altieri, K., Arrigo, K. R., Baker, A. R., Capone, D. G., Cornell, S.,
9 Dentener, F., Galloway, J., Ganeshram, R. S., Geider, R. J., Jickells, T., Kuypers, M. M.,
10 Langlois, R., Liss, P. S., Liu, S. M., Middelburg, J. J., Moore, C. M., Nickovic, S., Oschlies,
11 A., Pedersen, T., Prospero, J., Schlitzer, R., Seitzinger, S., Sorensen, L. L., Uematsu, M.,
12 Ulloa, O., Voss, M., Ward, B. and Zamora, L.: Impacts of atmospheric anthropogenic
13 nitrogen on the open ocean., *Science*, 320(5878), 893–7, doi:10.1126/science.1150369, 2008.
- 14 Duncan, B. N., Yoshida, Y., de Foy, B., Lamsal, L. N., Streets, D. G., Lu, Z., Pickering, K. E.
15 and Krotkov, N. A.: The observed response of Ozone Monitoring Instrument (OMI) NO₂
16 columns to NO_x emission controls on power plants in the United States: 2005–2011, *Atmos.*
17 *Environ.*, 81, 102–111, doi:10.1016/j.atmosenv.2013.08.068, 2013.
- 18 Ellis, R. A., Jacob, D. J., Sulprizio, M. P., Zhang, L., Holmes, C. D., Schichtel, B. A., Blett,
19 T., Porter, E., Pardo, L. H. and Lynch, J. A.: Present and future nitrogen deposition to national
20 parks in the United States: critical load exceedances, *Atmos. Chem. Phys.*, 13(17), 9083–
21 9095, doi:10.5194/acp-13-9083-2013, 2013.
- 22 Evans, M. J. and Jacob, D. J.: Impact of new laboratory studies of N₂O₅ hydrolysis on
23 global model budgets of tropospheric nitrogen oxides, ozone, and OH, *Geophys. Res. Lett.*,
24 32(9), L09813, doi:10.1029/2005GL022469, 2005.
- 25 Fountoukis, C. and Nenes, A.: ISORROPIA II: a computationally efficient thermodynamic
26 equilibrium model for K⁺-Ca²⁺-Mg²⁺-NH₄⁽⁺⁾-Na⁺-SO₄²⁻-NO₃⁻-Cl⁻-H₂O aerosols,
27 *Atmos. Chem. Phys.*, 7(17), 4639–4659, 2007.
- 28 Fowler, D., Muller, J., Smith, R. I., Cape, J. N. and Erisman, J. W.: Nonlinearities in source
29 receptor relationships for sulfur and nitrogen compounds., *Ambio*, 34(1), 41–6, 2005.
- 30 de Foy, B., Lu, Z. and Streets, D. G.: Satellite NO₂ retrievals suggest China has exceeded its
31 NO_x reduction goals from the twelfth Five-Year Plan, *Sci. Rep.*, 6, doi:10.1038/srep35912,



- 1 2016.
- 2 Galloway, J. N., Dentener, F. J., Capone, D. G., Boyer, E. W., Howarth, R. W., Seitzinger, S.
- 3 P., Asner, G. P., Cleveland, C. C., Green, P. A., Holland, E. A., Karl, D. M., Michaels, A. F.,
- 4 Porter, J. H., Townsend, A. R. and Vorosmarty, C. J.: Nitrogen cycles: past, present, and
- 5 future, *Biogeochemistry*, 70(2), 153–226, 2004.
- 6 Galloway, J. N., Townsend, A. R., Erisman, J. W., Bekunda, M., Cai, Z., Freney, J. R.,
- 7 Martinelli, L. A., Seitzinger, S. P. and Sutton, M. A.: Transformation of the Nitrogen Cycle:
- 8 Recent Trends, Questions, and Potential Solutions, *Science* (80-.), 320(5878), 2008.
- 9 Geddes, J. A., Martin, R. V., Boys, B. L. and van Donkelaar, A.: Long-Term Trends
- 10 Worldwide in Ambient NO₂ Concentrations Inferred from Satellite Observations, *Environ.*
- 11 *Health Perspect.*, 124(3), doi:10.1289/ehp.1409567, 2015.
- 12 Guenther, A., Karl, T., Harley, P., Wiedinmyer, C., Palmer, P. I. and Geron, C.: Estimates of
- 13 global terrestrial isoprene emissions using MEGAN (Model of Emissions of Gases and
- 14 Aerosols from Nature), *Atmos. Chem. Phys.*, 6, 3181–3210, 2006.
- 15 Hernández, D. L., Vallano, D. M., Zavaleta, E. S., Tzankova, Z., Pasari, J. R., Weiss, S.,
- 16 Selmants, P. C. and Morozumi, C.: Nitrogen Pollution Is Linked to US Listed Species
- 17 Declines, *Bioscience*, 66(3), 213–222, doi:10.1093/biosci/biw003, 2016.
- 18 Hilboll, A., Richter, A. and Burrows, J. P.: Long-term changes of tropospheric NO₂ over
- 19 megacities derived from multiple satellite instruments, *Atmos. Chem. Phys.*, 13(8), 4145–
- 20 4169, doi:10.5194/acp-13-4145-2013, 2013.
- 21 Holland, E. A., Braswell, B. H., Sulzman, J. and Lamarque, J. F.: Nitrogen deposition onto
- 22 the United States and western Europe: Synthesis of observations and models, *Ecol. Appl.*,
- 23 15(1), 38–57, doi:10.1890/03-5162, 2005.
- 24 HTAP: Hemispheric Transport of Air Pollution 2010 - Part A: Ozone and Particulate Matter,
- 25 New York. [online] Available from: <http://www.htap.org/>, 2010.
- 26 Hu, C., Li, D., Chen, C., Ge, J., Muller-Karger, F. E., Liu, J., Yu, F. and He, M.-X.: On the
- 27 recurrent *Ulva prolifera* blooms in the Yellow Sea and East China Sea, *J. Geophys. Res.*,
- 28 115(C5), C05017, doi:10.1029/2009JC005561, 2010.
- 29 Hu, L., Millet, D. B., Baasandorj, M., Griffis, T. J., Travis, K. R., Tessum, C. W., Marshall, J.
- 30 D., Reinhart, W. F., Mikoviny, T., Müller, M., Wisthaler, A., Graus, M., Warneke, C. and de



- 1 Gouw, J.: Emissions of C6 -C8 aromatic compounds in the United States: Constraints from
2 tall tower and aircraft measurements, *J. Geophys. Res. Atmos.*, 120(2), 826–842,
3 doi:10.1002/2014JD022627, 2015.
- 4 Hudman, R. C., Moore, N. E., Mebust, A. K., Martin, R. V, Russell, A. R., Valin, L. C. and
5 Cohen, R. C.: Steps towards a mechanistic model of global soil nitric oxide emissions:
6 implementation and space based-constraints, *Atmos. Chem. Phys.*, 12(16), 7779–7795,
7 doi:10.5194/acp-12-7779-2012, 2012.
- 8 Isbell, F., Reich, P. B., Tilman, D., Hobbie, S. E., Polasky, S. and Binder, S.: Nutrient
9 enrichment, biodiversity loss, and consequent declines in ecosystem productivity., *Proc. Natl.*
10 *Acad. Sci. U. S. A.*, 110(29), 11911–6, doi:10.1073/pnas.1310880110, 2013.
- 11 Jacob, D. J.: Heterogeneous chemistry and tropospheric ozone, *Atmos. Environ.*, 34(12),
12 2131–2159, doi:10.1016/S1352-2310(99)00462-8, 2000.
- 13 Jaegle, L., Steinberger, L., Martin, R. V and Chance, K.: Global partitioning of NO_x sources
14 using satellite observations: Relative roles of fossil fuel combustion, biomass burning and soil
15 emissions, *Faraday Discuss.*, 130, 407–423, doi:10.1039/b502128f, 2005.
- 16 Jia, Y., Yu, G., Gao, Y., He, N., Wang, Q., Jiao, C. and Zuo, Y.: Global inorganic nitrogen
17 dry deposition inferred from ground- and space-based measurements., *Sci. Rep.*, 6, 19810,
18 doi:10.1038/srep19810, 2016.
- 19 Kanakidou, M., Myriokefalitakis, S., Daskalakis, N., Fanourgakis, G., Nenes, A., Baker, A.
20 R., Tsigaridis, K., Mihalopoulos, N., Kanakidou, M., Myriokefalitakis, S., Daskalakis, N.,
21 Fanourgakis, G., Nenes, A., Baker, A. R., Tsigaridis, K. and Mihalopoulos, N.: Past, Present,
22 and Future Atmospheric Nitrogen Deposition, *J. Atmos. Sci.*, 73(5), 2039–2047,
23 doi:10.1175/JAS-D-15-0278.1, 2016.
- 24 Kendall, M. G.: Rank Correlation Methods, 4th ed., Charles Griffen, London., 1975.
- 25 Konovalov, I. B., Beekmann, M., Burrows, J. P. and Richter, A.: Satellite measurement based
26 estimates of decadal changes in European nitrogen oxides emissions, *Atmos. Chem. Phys.*,
27 8(10), 2623–2641, doi:10.5194/acp-8-2623-2008, 2008.
- 28 Konovalov, I. B., Beekmann, M., Richter, A., Burrows, J. P. and Hilboll, A.: Multi-annual
29 changes of NO_x emissions in megacity regions: nonlinear trend analysis of satellite
30 measurement based estimates, *Atmos. Chem. Phys.*, 10(17), 8481–8498, doi:10.5194/acp-10-



- 1 8481-2010, 2010.
- 2 Krotkov, N. A., McLinden, C. A., Li, C., Lamsal, L. N., Celarier, E. A., Marchenko, S. V.,
3 Swartz, W. H., Bucsela, E. J., Joiner, J., Duncan, B. N., Boersma, K. F., Veefkind, J. P.,
4 Levelt, P. F., Fioletov, V. E., Dickerson, R. R., He, H., Lu, Z. and Streets, D. G.: Aura OMI
5 observations of regional SO₂ and NO₂; pollution changes from 2005 to 2015, Atmos. Chem.
6 Phys., 16(7), 4605–4629, doi:10.5194/acp-16-4605-2016, 2016.
- 7 Kuhns, H., Knipping, E. M. and Vukovich, J. M.: Development of a United States-Mexico
8 Emissions Inventory for the Big Bend Regional Aerosol and Visibility Observational
9 (BRAVO) Study., J. Air Waste Manag. Assoc., 55(5), 677–92, 2005.
- 10 Lamarque, J.-F., Dentener, F., McConnell, J., Ro, C.-U., Shaw, M., Vet, R., Bergmann, D.,
11 Cameron-Smith, P., Dalsoren, S., Doherty, R., Faluvegi, G., Ghan, S. J., Josse, B., Lee, Y. H.,
12 MacKenzie, I. A., Plummer, D., Shindell, D. T., Skeie, R. B., Stevenson, D. S., Strode, S.,
13 Zeng, G., Curran, M., Dahl-Jensen, D., Das, S., Fritzsche, D. and Nolan, M.: Multi-model
14 mean nitrogen and sulfur deposition from the Atmospheric Chemistry and Climate Model
15 Intercomparison Project (ACCMIP): evaluation of historical and projected future changes,
16 Atmos. Chem. Phys., 13(16), 7997–8018, doi:10.5194/acp-13-7997-2013, 2013.
- 17 Lamsal, L. N., Martin, R. V., van Donkelaar, A., Celarier, E. A., Bucsela, E. J., Boersma, K.
18 F., Dirksen, R., Luo, C. and Wang, Y.: Indirect validation of tropospheric nitrogen dioxide
19 retrieved from the OMI satellite instrument: Insight into the seasonal variation of nitrogen
20 oxides at northern midlatitudes, J. Geophys. Res., 115(D5), D05302,
21 doi:10.1029/2009JD013351, 2010.
- 22 Lamsal, L. N., Martin, R. V., Padmanabhan, A., Van Donkelaar, A., Zhang, Q., Sioris, C. E.,
23 Chance, K., Kurosu, T. P. and Newchurch, M. J.: Application of satellite observations for
24 timely updates to global anthropogenic NO_x emission inventories, Geophys. Res. Lett., 38(5),
25 2011.
- 26 Lee, H.-J., Kim, S.-W., Brioude, J., Cooper, O. R., Frost, G. J., Kim, C.-H., Park, R. J.,
27 Trainer, M. and Woo, J.-H.: Transport of NO_x in East Asia identified by satellite and in situ
28 measurements and Lagrangian particle dispersion model simulations, J. Geophys. Res.
29 Atmos., 119(5), 2574–2596, doi:10.1002/2013JD021185, 2014.
- 30 Lee, H.-M., Paulot, F., Henze, D. K., Travis, K., Jacob, D. J., Pardo, L. H. and Schichtel, B.
31 A.: Sources of nitrogen deposition in Federal Class I areas in the US, Atmos. Chem. Phys.,



- 1 16(2), 525–540, doi:10.5194/acp-16-525-2016, 2016.
- 2 Li, Y., Schichtel, B. A., Walker, J. T., Schwede, D. B., Chen, X., Lehmann, C. M. B.,
3 Puchalski, M. A., Gay, D. A. and Collett, J. L.: Increasing importance of deposition of
4 reduced nitrogen in the United States., *Proc. Natl. Acad. Sci. U. S. A.*, 113(21), 5874–9,
5 doi:10.1073/pnas.1525736113, 2016.
- 6 Lin, M., Oki, T., Bengtsson, M., Kanae, S., Holloway, T. and Streets, D. G.: Long-range
7 transport of acidifying substances in East Asia—Part II: Source–receptor relationships,
8 *Atmos. Environ.*, 42(24), 5956–5967, doi:10.1016/j.atmosenv.2008.03.039, 2008.
- 9 Liu, H., Jacob, D. J., Bey, I. and Yantosca, R. M.: Constraints from 210 Pb and 7 Be on wet
10 deposition and transport in a global three-dimensional chemical tracer model driven by
11 assimilated meteorological fields, *J. Geophys. Res. Atmos.*, 106(D11), 12109–12128,
12 doi:10.1029/2000JD900839, 2001.
- 13 Liu, L. L. and Greaver, T. L.: A review of nitrogen enrichment effects on three biogenic
14 GHGs: the CO₂ sink may be largely offset by stimulated N₂O and CH₄ emission, *Ecol. Lett.*,
15 12(10), 1103–1117, 2009.
- 16 Lu, X., Jiang, H., Zhang, X., Liu, J., Zhang, Z., Jin, J., Wang, Y., Xu, J. and Cheng, M.:
17 Estimated global nitrogen deposition using NO₂ column density, *Int. J. Remote Sens.*, 34(24),
18 8893–8906, doi:10.1080/01431161.2013.853894, 2013.
- 19 Lu, Z., Streets, D. G., De Foy, B., Lamsal, L. N., Duncan, B. N. and Xing, J.: Emissions of
20 nitrogen oxides from US urban areas: Estimation from Ozone Monitoring Instrument
21 retrievals for 2005–2014, *Atmos. Chem. Phys.*, 15(18), 10367–10383, doi:10.5194/acp-15-
22 10367-2015, 2015.
- 23 Mann, H. B.: Non-parametric tests against trend, *Econometrica*, 13, 163–171, 1945.
- 24 Mao, J., Fan, S., Jacob, D. J. and Travis, K. R.: Radical loss in the atmosphere from Cu-Fe
25 redox coupling in aerosols, *Atmos. Chem. Phys.*, 13(2), 509–519, doi:10.5194/acp-13-509-
26 2013, 2013.
- 27 Martin, R. V.: Global inventory of nitrogen oxide emissions constrained by space-based
28 observations of NO₂ columns, *J. Geophys. Res.*, 108(D17), 4537,
29 doi:10.1029/2003JD003453, 2003.
- 30 Martin, R. V., Jacob, D. J., Yantosca, R. M., Chin, M. and Ginoux, P.: Global and regional



- 1 decreases in tropospheric oxidants from photochemical effects of aerosols, *J. Geophys. Res.*
2 *Atmos.*, 108(D3), n/a-n/a, doi:10.1029/2002JD002622, 2003.
- 3 McLinden, C. A., Fioletov, V., Boersma, K. F., Krotkov, N., Sioris, C. E., Veefkind, J. P. and
4 Yang, K.: Air quality over the Canadian oil sands: A first assessment using satellite
5 observations, *Geophys. Res. Lett.*, 39(4), n/a-n/a, doi:10.1029/2011GL050273, 2012.
- 6 Mijling, B., van der A, R. J. and Zhang, Q.: Regional nitrogen oxides emission trends in East
7 Asia observed from space, *Atmos. Chem. Phys.*, 13(23), 12003–12012, doi:10.5194/acp-13-
8 12003-2013, 2013.
- 9 Miyazaki, K., Eskes, H., Sudo, K., Boersma, K. F., Bowman, K. and Kanaya, Y.: Decadal
10 changes in global surface NO_x emissions from multi-constituent satellite data assimilation,
11 *Atmos. Chem. Phys. Discuss.*, 1–48, doi:10.5194/acp-2016-529, 2016.
- 12 Morino, Y., Ohara, T., Kurokawa, J., Kuribayashi, M., Uno, I. and Hara, H.: Temporal
13 variations of nitrogen wet deposition across Japan from 1989 to 2008, *J. Geophys. Res.*,
14 116(D6), D06307, doi:10.1029/2010JD015205, 2011.
- 15 Mu, M., Randerson, J. T., van der Werf, G. R., Giglio, L., Kasibhatla, P., Morton, D., Collatz,
16 G. J., DeFries, R. S., Hyer, E. J., Prins, E. M., Griffith, D. W. T., Wunch, D., Toon, G. C.,
17 Sherlock, V. and Wennberg, P. O.: Daily and 3-hourly variability in global fire emissions and
18 consequences for atmospheric model predictions of carbon monoxide, *J. Geophys. Res.*
19 *Atmos.*, 116(D24), n/a-n/a, doi:10.1029/2011JD016245, 2011.
- 20 Murray, L. T., Jacob, D. J., Logan, J. A., Hudman, R. C. and Koshak, W. J.: Optimized
21 regional and interannual variability of lightning in a global chemical transport model
22 constrained by LIS/OTD satellite data, *J. Geophys. Res. Atmos.*, 117(D20), n/a-n/a,
23 doi:10.1029/2012JD017934, 2012.
- 24 Neuman, J. A., Parrish, D. D., Trainer, M., Ryerson, T. B., Holloway, J. S., Nowak, J. B.,
25 Swanson, A., Flocke, F., Roberts, J. M., Brown, S. S., Stark, H., Sommariva, R., Stohl, A.,
26 Peltier, R., Weber, R., Wollny, A. G., Sueper, D. T., Hubler, G. and Fehsenfeld, F. C.:
27 Reactive nitrogen transport and photochemistry in urban plumes over the North Atlantic
28 Ocean, *J. Geophys. Res. Atmos.*, 111(D23), doi:10.1029/2005JD007010, 2006.
- 29 Nowlan, C. R., Martin, R. V., Philip, S., Lamsal, L. N., Krotkov, N. A., Marais, E. A., Wang,
30 S. and Zhang, Q.: Global dry deposition of nitrogen dioxide and sulfur dioxide inferred from
31 space-based measurements, *Global Biogeochem. Cycles*, n/a-n/a,



- 1 doi:10.1002/2014GB004805, 2014.
- 2 Olivier, J. G. J., Van Aardenne, J. A., Dentener, F. J., Pagliari, V., Ganzeveld, L. N. and
3 Peters, J. A. H. W.: Recent trends in global greenhouse gas emissions: regional trends 1970–
4 2000 and spatial distribution of key sources in 2000, *Environ. Sci.*, 2(2–3), 81–99,
5 doi:10.1080/15693430500400345, 2005.
- 6 Park, R. J., Jacob, D. J., Field, B. D. and Yantosca, R. M.: Natural and transboundary
7 pollution influences on sulfate-nitrate-ammonium aerosols in the United States: Implications
8 for policy, *J. Geophys. Res.*, 109(D15), D15204, doi:10.1029/2003JD004473, 2004.
- 9 Paulot, F., Crouse, J. D., Kjaergaard, H. G., Kroll, J. H., Seinfeld, J. H. and Wennberg, P. O.:
10 Isoprene photooxidation: new insights into the production of acids and organic nitrates,
11 *Atmos. Chem. Phys.*, 9(4), 1479–1501, 2009a.
- 12 Paulot, F., Crouse, J. D., Kjaergaard, H. G., Kürten, A., St Clair, J. M., Seinfeld, J. H. and
13 Wennberg, P. O.: Unexpected epoxide formation in the gas-phase photooxidation of
14 isoprene., *Science*, 325(5941), 730–3, doi:10.1126/science.1172910, 2009b.
- 15 Reay, D. S., Dentener, F., Smith, P., Grace, J. and Feely, R. A.: Global nitrogen deposition
16 and carbon sinks, *Nat. Geosci.*, 1(7), 430–437, 2008.
- 17 Reis, S., Pinder, R. W., Zhang, M., Lijie, G. and Sutton, M. A.: Reactive nitrogen in
18 atmospheric emission inventories, *Atmos. Chem. Phys.*, 9(19), 7657–7677, doi:10.5194/acp-
19 9-7657-2009, 2009.
- 20 Richter, A., Eyring, V., Burrows, J. P., Bovensmann, H., Lauer, A., Sierk, B. and Crutzen, P.
21 J.: Satellite measurements of NO₂ from international shipping emissions, *Geophys. Res.*
22 *Lett.*, 31(23), doi:10.1029/2004GL020822, 2004.
- 23 Richter, A., Burrows, J. P., Nüss, H., Granier, C. and Niemeier, U.: Increase in tropospheric
24 nitrogen dioxide over China observed from space., *Nature*, 437(7055), 129–32,
25 doi:10.1038/nature04092, 2005.
- 26 Russell, A. R., Valin, L. C. and Cohen, R. C.: Trends in OMI NO₂ observations over the
27 United States: effects of emission control technology and the economic recession, *Atmos.*
28 *Chem. Phys.*, 12(24), 12197–12209, doi:10.5194/acp-12-12197-2012, 2012.
- 29 Sanderson, M. G., Dentener, F. J., Fiore, A. M., Cuvelier, C., Keating, T. J., Zuber, A.,
30 Atherton, C. S., Bergmann, D. J., Diehl, T., Doherty, R. M., Duncan, B. N., Hess, P.,



- 1 Horowitz, L. W., Jacob, D. J., Jonson, J. E., Kaminski, J. W., Lupu, A., MacKenzie, I. A.,
2 Mancini, E., Marmer, E., Park, R., Pitari, G., Prather, M. J., Pringle, K. J., Schroeder, S.,
3 Schultz, M. G., Shindell, D. T., Szopa, S., Wild, O. and Wind, P.: A multi-model study of the
4 hemispheric transport and deposition of oxidised nitrogen, *Geophys. Res. Lett.*, 35(17), 2008.
- 5 De Schrijver, A., De Frenne, P., Ampoorter, E., Van Nevel, L., Demey, A., Wuyts, K. and
6 Verheyen, K.: Cumulative nitrogen input drives species loss in terrestrial ecosystems, *Glob.*
7 *Ecol. Biogeogr.*, 20(6), 803–816, doi:10.1111/j.1466-8238.2011.00652.x, 2011.
- 8 Sen, P. K.: Estimates of the Regression Coefficient Based on Kendall's Tau, *J. Am. Stat.*
9 *Assoc.*, 63(324), 1379–1389, doi:10.1080/01621459.1968.10480934, 1968.
- 10 Sickles II, J. E. and Shadwick, D. S.: Changes in air quality and atmospheric deposition in the
11 eastern United States: 1990–2004, *J. Geophys. Res.*, 112(D17), D17301,
12 doi:10.1029/2006JD007843, 2007.
- 13 Sickles II, J. E. and Shadwick, D. S.: Air quality and atmospheric deposition in the eastern
14 US: 20 years of change, *Atmos. Chem. Phys.*, 15(1), 173–197, doi:10.5194/acp-15-173-2015,
15 2015.
- 16 Souri, A. H., Choi, Y., Jeon, W., Li, X., Pan, S., Diao, L. and Westenbarger, D. A.:
17 Constraining NO_x emissions using satellite NO₂ measurements during 2013 DISCOVER-AQ
18 Texas campaign, *Atmos. Environ.*, 131, 371–381, doi:10.1016/j.atmosenv.2016.02.020, 2016.
- 19 Stavrakou, T., Müller, J.-F., Boersma, K. F., De Smedt, I. and van der A, R. J.: Assessing the
20 distribution and growth rates of NO_x emission sources by inverting a 10-year record of NO₂
21 satellite columns, *Geophys. Res. Lett.*, 35(10), L10801, doi:10.1029/2008GL033521, 2008.
- 22 Stettler, M. E. J., Eastham, S. and Barrett, S. R. H.: Air quality and public health impacts of
23 UK airports. Part I: Emissions, *Atmos. Environ.*, 45(31), 5415–5424,
24 doi:10.1016/j.atmosenv.2011.07.012, 2011.
- 25 Streets, D. G., Canty, T., Carmichael, G. R., de Foy, B., Dickerson, R. R., Duncan, B. N.,
26 Edwards, D. P., Haynes, J. A., Henze, D. K., Houyoux, M. R., Jacob, D. J., Krotkov, N. A.,
27 Lamsal, L. N., Liu, Y., Lu, Z., Martin, R. V., Pfister, G. G., Pinder, R. W., Salawitch, R. J.
28 and Wecht, K. J.: Emissions estimation from satellite retrievals: A review of current
29 capability, *Atmos. Environ.*, 77, 1011–1042, doi:10.1016/j.atmosenv.2013.05.051, 2013.
- 30 Tanimoto, H., Sawa, Y., Matsueda, H., Uno, I., Ohara, T., Yamaji, K., Kurokawa, J. and



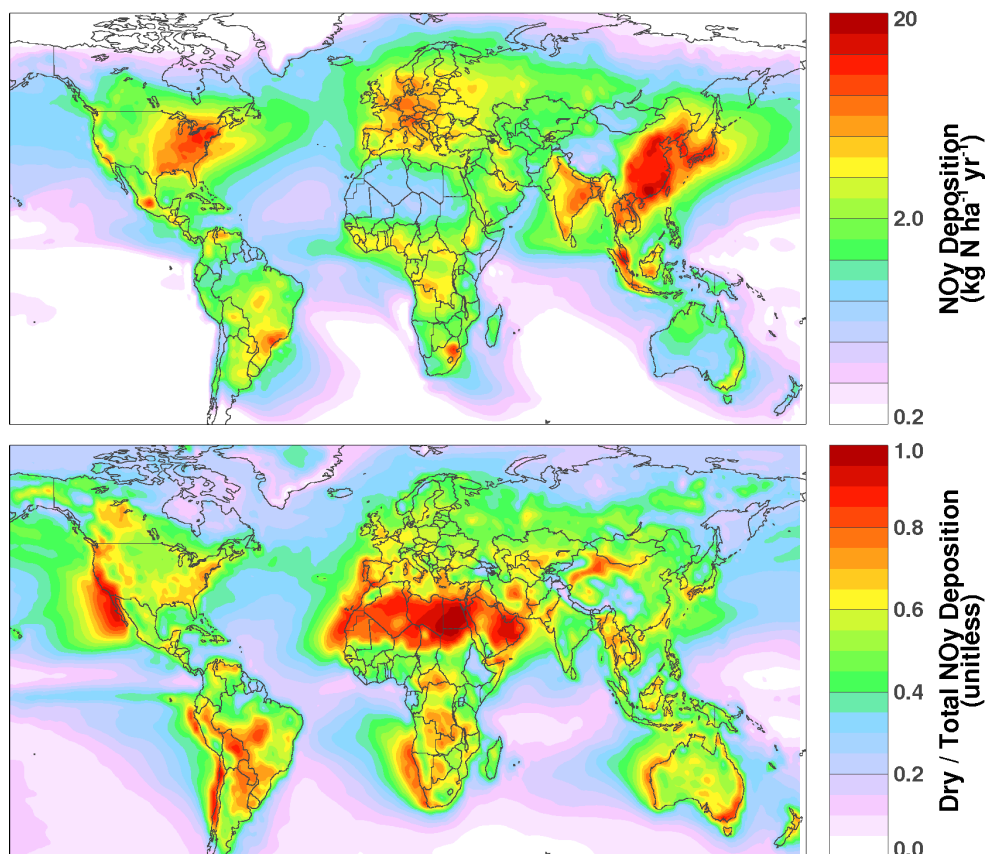
- 1 Yonemura, S.: Significant latitudinal gradient in the surface ozone spring maximum over East
2 Asia, *Geophys. Res. Lett.*, 32(21), L21805, doi:10.1029/2005GL023514, 2005.
- 3 Templer, P. H., Pinder, R. W. and Goodale, C. L.: Effects of nitrogen deposition on
4 greenhouse-gas fluxes for forests and grasslands of North America, *Front. Ecol. Environ.*,
5 10(10), 547–553, doi:10.1890/120055, 2012.
- 6 Valin, L. C., Russell, a. R., Hudman, R. C. and Cohen, R. C.: Effects of model resolution on
7 the interpretation of satellite NO₂ observations, *Atmos. Chem. Phys.*, 11(22), 11647–11655,
8 doi:10.5194/acp-11-11647-2011, 2011.
- 9 Veefkind, J. P., Aben, I., McMullan, K., Förster, H., de Vries, J., Otter, G., Claas, J., Eskes,
10 H. J., de Haan, J. F., Kleipool, Q., van Weele, M., Hasekamp, O., Hoogeveen, R., Landgraf,
11 J., Snel, R., Tol, P., Ingmann, P., Voors, R., Kruizinga, B., Vink, R., Visser, H. and Levelt, P.
12 F.: TROPOMI on the ESA Sentinel-5 Precursor: A GMES mission for global observations of
13 the atmospheric composition for climate, air quality and ozone layer applications, *Remote
14 Sens. Environ.*, 120, 70–83, doi:10.1016/j.rse.2011.09.027, 2012.
- 15 Vet, R., Artz, R. S., Carou, S., Shaw, M., Ro, C.-U., Aas, W., Baker, A., Bowersox, V. C.,
16 Dentener, F., Galy-Lacaux, C., Hou, A., Pienaar, J. J., Gillett, R., Forti, M. C., Gromov, S.,
17 Hara, H., Khodzher, T., Mahowald, N. M., Nickovic, S., Rao, P. S. P. and Reid, N. W.: A
18 global assessment of precipitation chemistry and deposition of sulfur, nitrogen, sea salt, base
19 cations, organic acids, acidity and pH, and phosphorus, *Atmos. Environ.*, 93, 3–100,
20 doi:10.1016/j.atmosenv.2013.10.060, 2014.
- 21 Vinken, G. C. M., Boersma, K. F., Maasakkers, J. D., Adon, M. and Martin, R. V.:
22 Worldwide biogenic soil NO_x emissions inferred from OMI NO₂ observations, *Atmos.
23 Chem. Phys. Discuss.*, 14(10), 14683–14724, doi:10.5194/acpd-14-14683-2014, 2014.
- 24 Walker, T. W., Martin, R. V., van Donkelaar, A., Leaitch, W. R., MacDonald, A. M., Anlauf,
25 K. G., Cohen, R. C., Bertram, T. H., Huey, L. G., Avery, M. A., Weinheimer, A. J., Flocke, F.
26 M., Tarasick, D. W., Thompson, A. M., Streets, D. G. and Liu, X.: Trans-Pacific transport of
27 reactive nitrogen and ozone to Canada during spring, *Atmos. Chem. Phys.*, 10(17), 8353–
28 8372, doi:10.5194/acp-10-8353-2010, 2010.
- 29 Wang, Y. H., Jacob, D. J. and Logan, J. A.: Global simulation of tropospheric O₃-NO_x-
30 hydrocarbon chemistry 1. Model formulation, *J. Geophys. Res.*, 103(D9), 10713–10725,
31 doi:10.1029/98JD00158, 1998.



- 1 Wesely, M. L.: Parameterization of surface resistances to gaseous dry deposition in regional-
2 scale numerical models, *Atmos. Environ.*, 23(6), 1293–1304, doi:10.1016/0004-
3 6981(89)90153-4, 1989.
- 4 World Health Organization: WHO Air Quality Guidelines for Europe, 2nd edition, [online]
5 Available from: [http://www.euro.who.int/en/publications/abstracts/air-quality-guidelines-for-](http://www.euro.who.int/en/publications/abstracts/air-quality-guidelines-for-europe)
6 [europe](http://www.euro.who.int/en/publications/abstracts/air-quality-guidelines-for-europe) (Accessed 28 October 2016), 2000.
- 7 Zbieranowski, A. L. and Aherne, J.: Long-term trends in atmospheric reactive nitrogen across
8 Canada: 1988–2007, *Atmos. Environ.*, 45(32), 5853–5862,
9 doi:10.1016/j.atmosenv.2011.06.080, 2011.
- 10 Zhang, L., Gong, S., Padro, J. and Barrie, L.: A size-segregated particle dry deposition
11 scheme for an atmospheric aerosol module, *Atmos. Environ.*, 35(3), 549–560,
12 doi:10.1016/S1352-2310(00)00326-5, 2001.
- 13 Zhang, L., Jacob, D. J., Boersma, K. F., Jaffe, D. A., Olson, J. R., Bowman, K. W., Worden,
14 J. R., Thompson, A. M., Avery, M. A., Cohen, R. C., Dibb, J. E., Flock, F. M., Fuelberg, H.
15 E., Huey, L. G., McMillan, W. W., Singh, H. B. and Weinheimer, A. J.: Transpacific
16 transport of ozone pollution and the effect of recent Asian emission increases on air quality in
17 North America: an integrated analysis using satellite, aircraft, ozonesonde, and surface
18 observations, *Atmos. Chem. Phys.*, 8(20), 6117–6136, doi:10.5194/acp-8-6117-2008, 2008.
- 19 Zhang, L., Jacob, D. J., Knipping, E. M., Kumar, N., Munger, J. W., Carouge, C. C., Van
20 Donkelaar, A., Wang, Y. X. and Chen, D.: Nitrogen deposition to the United States:
21 Distribution, sources, and processes, *Atmos. Chem. Phys.*, 12(10), 4539–4554, 2012.
- 22 Zhang, Q., Streets, D. G., He, K., Wang, Y., Richter, A., Burrows, J. P., Uno, I., Jang, C. J.,
23 Chen, D., Yao, Z. and Lei, Y.: NO_x emission trends for China, 1995–2004: The view from
24 the ground and the view from space, *J. Geophys. Res.*, 112(D22), D22306,
25 doi:10.1029/2007JD008684, 2007.
- 26 Zhang, Q., Streets, D. G., Carmichael, G. R., He, K. B., Huo, H., Kannari, A., Klimont, Z.,
27 Park, I. S., Reddy, S., Fu, J. S., Chen, D., Duan, L., Lei, Y., Wang, L. T. and Yao, Z. L.:
28 Asian emissions in 2006 for the NASA INTEX-B mission, *Atmos. Chem. Phys.*, 9(14), 5131–
29 5153, doi:10.5194/acp-9-5131-2009, 2009.
- 30 Zhao, Y., Zhang, L., Pan, Y., Wang, Y., Paulot, F. and Henze, D. K.: Atmospheric nitrogen
31 deposition to the northwestern Pacific: seasonal variation and source attribution, *Atmos.*



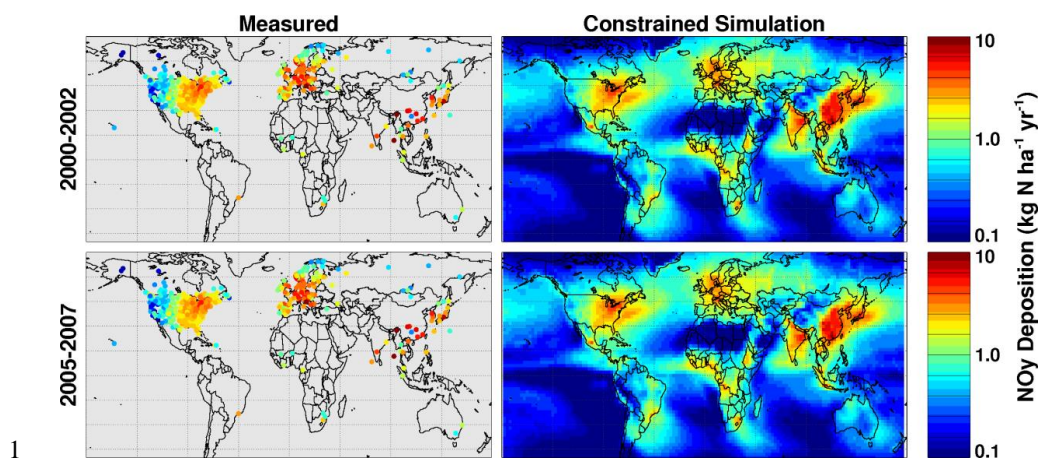
- 1 Chem. Phys., 15(18), 10905–10924, doi:10.5194/acp-15-10905-2015, 2015.
- 2 Zien, A. W., Richter, A., Hilboll, A., Blechschmidt, A.-M. and Burrows, J. P.: Systematic
3 analysis of tropospheric NO₂ long-range transport events detected in GOME-2 satellite data,
4 Atmos. Chem. Phys., 14(14), 7367–7396, doi:10.5194/acp-14-7367-2014, 2014.
- 5 Zoogman, P., Liu, X., Suleiman, R. M., Pennington, W. F., Flittner, D. E., Al-Saadi, J. A.,
6 Hilton, B. B., Nicks, D. K., Newchurch, M. J., Carr, J. L., Janz, S. J., Andraschko, M. R.,
7 Arola, A., Baker, B. D., Canova, B. P., Chan Miller, C., Cohen, R. C., Davis, J. E., Dussault,
8 M. E., Edwards, D. P., Fishman, J., Ghulam, A., González Abad, G., Grutter, M., Herman, J.
9 R., Houck, J., Jacob, D. J., Joiner, J., Kerridge, B. J., Kim, J., Krotkov, N. A., Lamsal, L., Li,
10 C., Lindfors, A., Martin, R. V., McElroy, C. T., McLinden, C., Natraj, V., Neil, D. O.,
11 Nowlan, C. R., O'Sullivan, E. J., Palmer, P. I., Pierce, R. B., Pippin, M. R., Saiz-Lopez, A.,
12 Spurr, R. J. D., Szykman, J. J., Torres, O., Veefkind, J. P., Veihelmann, B., Wang, H., Wang,
13 J. and Chance, K.: Tropospheric emissions: Monitoring of pollution (TEMPO), J. Quant.
14 Spectrosc. Radiat. Transf., doi:10.1016/j.jqsrt.2016.05.008, 2016.
- 15
- 16



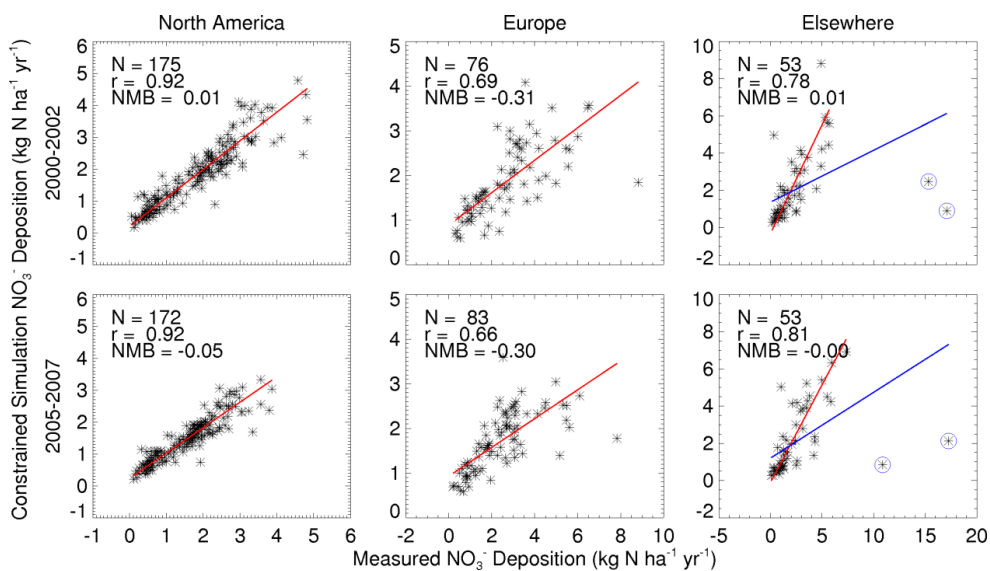
1

2 Figure 1: Long-term (1996-2014) mean NO_y deposition derived from the GEOS-Chem
3 simulation constrained by satellite observations of NO_2 columns from the GOME,
4 SCIAMACHY, and GOME-2 instruments (top). Mean ratio of simulated dry NO_y deposition
5 to total NO_y deposition (bottom).

6



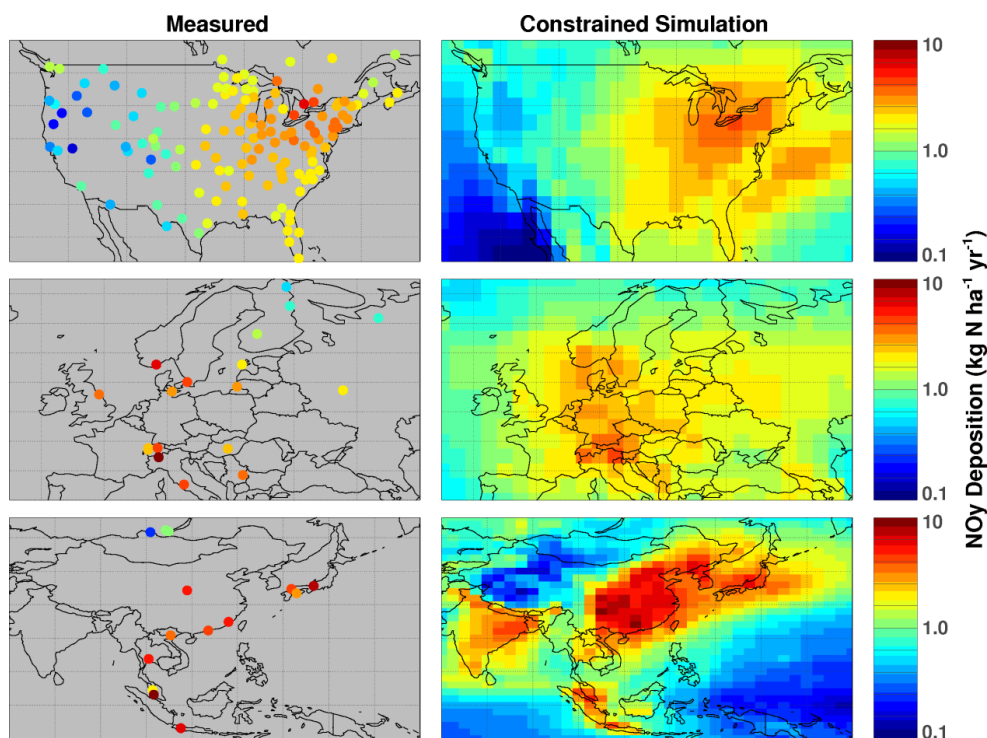
1
2 Figure 2: Annual wet NO₃⁻ deposition from measurements available through the World Data
3 Centre for Precipitation Chemistry, and from the GEOS-Chem simulation constrained with
4 satellite observations of NO₂. Two time periods are represented: 2000-2002 and 2005-2007.
5



1

2 Figure 3: Scatter plot of the satellite-constrained simulated wet NO_3^- deposition vs.
3 measurements available through the World Data Centre for Precipitation Chemistry for
4 specific subsets of the data. The red lines show the result of a reduced major axis linear
5 regression. In the right column, the blue line shows the fit across all data and the red line
6 shows the fit excluding the two circled data points that are discussed in the text (reported
7 statistics refer to the red line fit).

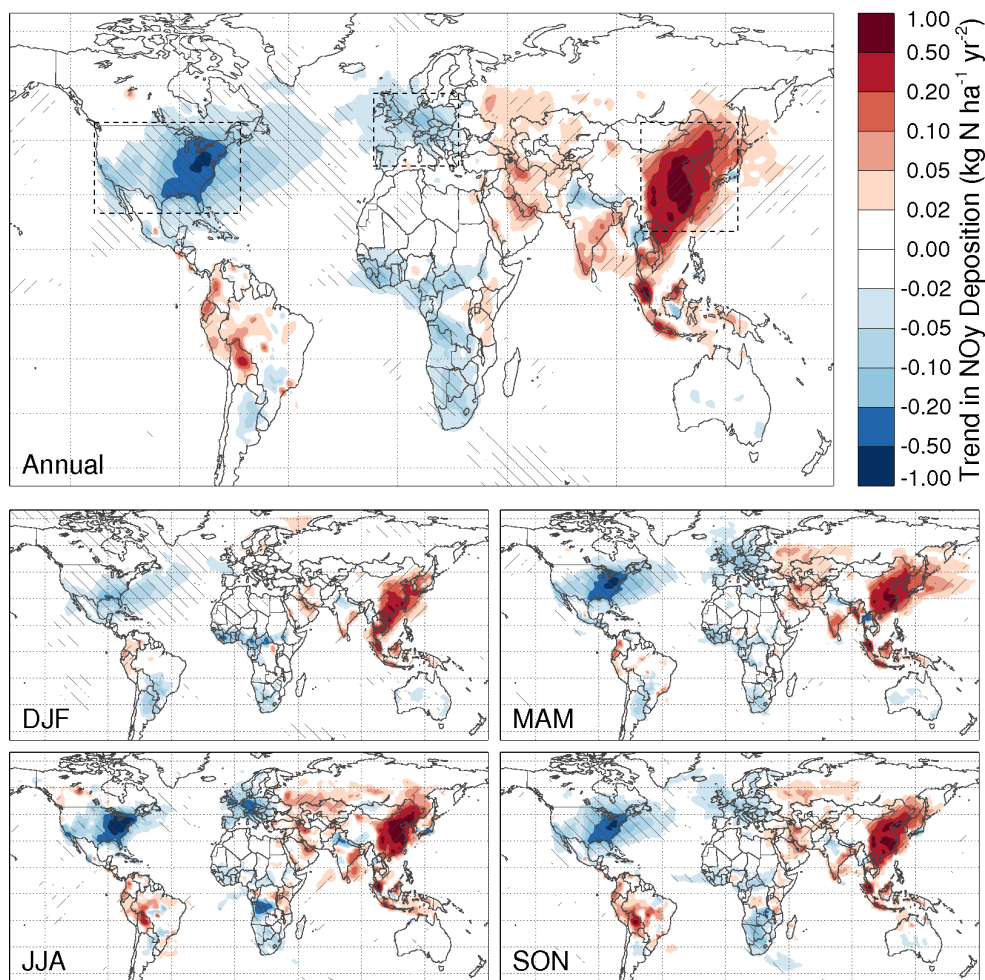
8



1

2 Figure 4: Long-term (1996-2014) wet NO_3^- deposition from available regional network
3 measurements (top: NADP and CAPMON; middle: EMEP; bottom: EANet), and from the
4 GEOS-Chem simulation constrained with satellite observations of NO_2 .

5

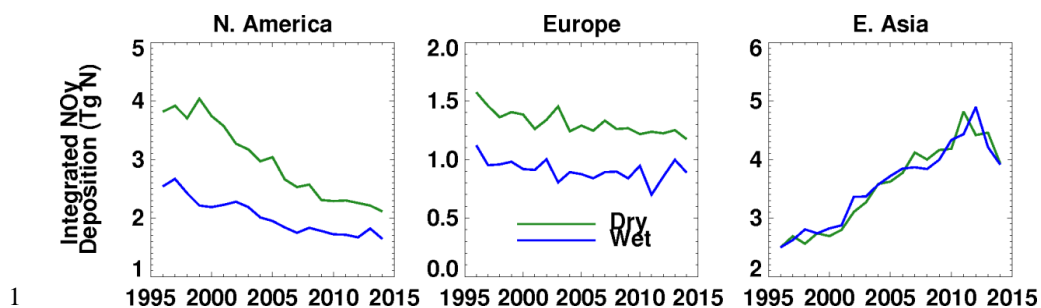


1

2 Figure 5. Long-term trend (1996-2014) in the satellite-constrained simulation of NO_y
3 deposition. (A) Annual mean; (B) December-January-February; (C) March-April-May; (D)
4 June-July-August; (E) September-October-November. Diagonal hatching represents trend
5 significance ($p < 0.01$). Hatching from top-left to bottom-right indicates a decreasing trend;
6 hatching from bottom-left to top-right indicates an increasing trend.

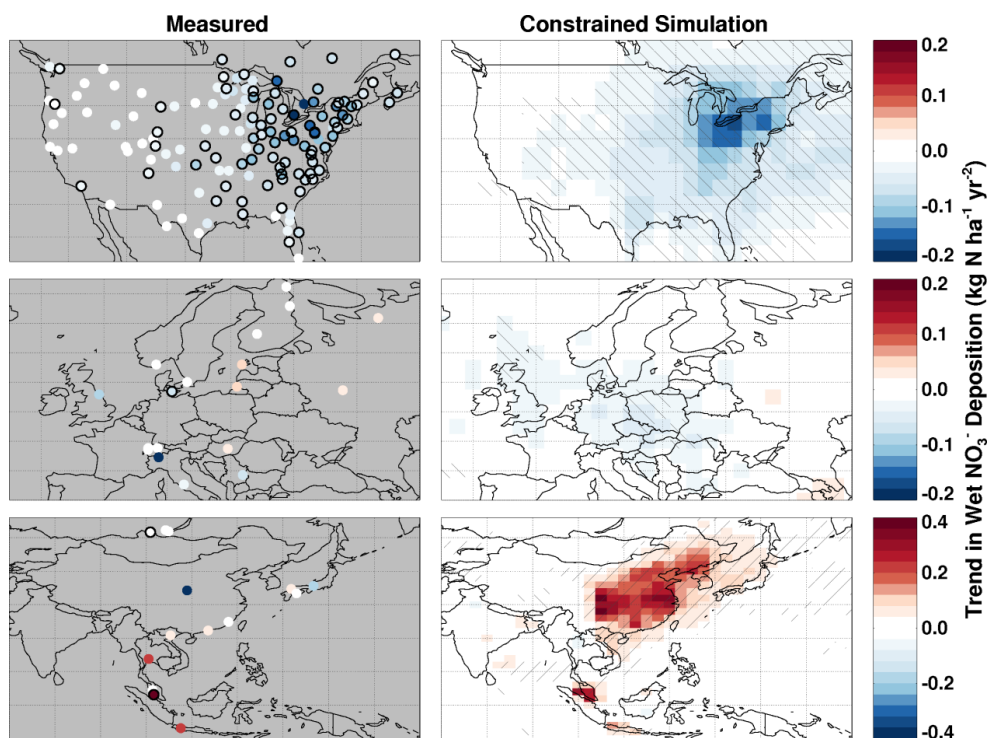
7

8



1
2 Figure 6: Timeseries of annually integrated dry and wet NO_y deposition over specific regions
3 (North America, Europe, and East Asia) as defined by the dashed rectangles in Figure 5.

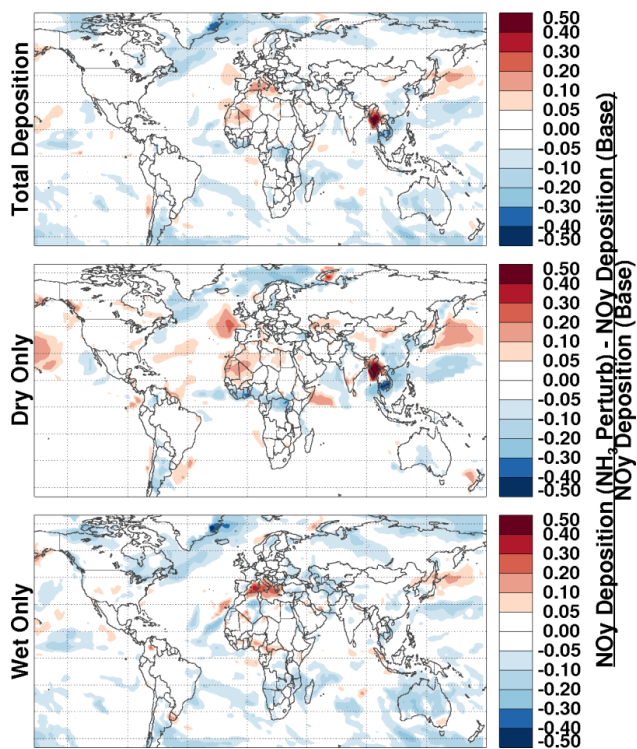
4
5



1

2 Figure 7: Long-term (1996-2014) trends in wet NO_3^- deposition from available regional
3 network measurements (as in Figure 4), and from the GEOS-Chem simulation constrained by
4 satellite observations of NO_2 . Closed circles around the measurements indicate significant
5 trends ($p < 0.01$); hatching indicates statistical significance in the simulation.

6



1

2 Figure 8: Sensitivity of simulated NO_y deposition to a 25% perturbation in ammonia
3 emissions in all grid boxes (shown separately for total deposition, dry deposition, and wet
4 deposition).